

An Improvement in Operation for Steel Rolling Mill Crop Cobble Shear using Direct Torque  
Control Induction Motor Drive

A Thesis

Presented in Partial Fulfillment of the Requirements for the

Degree of Master of Science

with a

Major in Electrical Engineering

in the

College of Graduate Studies

University of Idaho

by

Gary Ng

Major Professor: Herbert Hess Ph.D.

Committee Members: Michael Santora, Ph.D.; David Carpenter, Ph.D.

Department Administrator: Mohsen M. Guizani, Ph.D.

August 2015

### Authorization to Submit Thesis

This thesis of Gary Ng, submitted for the degree of Master of Science with a Major in Electrical Engineering and titled “An Improvement in Operation for Steel Rolling Mill Crop Cobble Shear using Direct Torque Control Induction Motor Drive,” has been reviewed in final form. Permission, as indicated by the signatures and dates below, is now granted to submit final copies to the College of Graduate Studies for approval.

Major Professor: \_\_\_\_\_ Date: \_\_\_\_\_  
Herbert Hess, Ph.D.

Committee Members \_\_\_\_\_ Date: \_\_\_\_\_  
Michael Santora, Ph.D.

\_\_\_\_\_ Date: \_\_\_\_\_  
David Carpenter, Ph.D.

Department \_\_\_\_\_ Date: \_\_\_\_\_  
Administrator: Mohsen M. Guizani, Ph.D.

## **Abstract**

The thesis describes how a Direct Torque Control (DTC) drive technology has been modified to provide improved control of a Crop Cobble Shear (CCS) system in a steel rolling mill. During the CCS cobble cutting mode, the original DTC drive experiences overcurrent faults that cause production downtimes. A model of the DTC induction motor drive system has been developed and this allowed the CCS operation to be analyzed and modified to improve performance. The simulated DTC induction motor drive is compared with the original existing system from a steel plant. Measurement data from the original system in the steel mill are favorably compared with simulation results. This comparison shows that the system has been successfully simulated to determine a suitable approach to improving the CCS operation. The real world modification of the CCS drive system is implemented successfully and proved to the overcurrent fault is eliminated.

## **Acknowledgements**

### **Major Professor – Dr. Herbert Hess**

I would also like to extend my deepest gratitude to Dr. Hess. Without his assistance and encouragement, I would not have a chance to even study the Master of Science program. He has been supportive and has given me the freedom to complete the master program during last 4 years. He has also provided insightful discussions, continuous support my master thesis and research with his patience, motivation, enthusiasm, and immense knowledge. His guidance helped me in all the time throughout the program. I could not have imagined having a better advisor and major professor for my graduate school. Dr. Hess is someone you will instantly respect and never forget once you know him. He is and remains my best role model as an engineer, scientist, mentor, and teacher.

### **Thesis Committee (Outside Member) – Dr. David Carpenter**

Besides my major professor, a special acknowledgement is necessary for Dr. Carpenter for his leadership, encouragement, insightful comments and helpful advices. He also spent countless hours on reviewing, providing invaluable suggestions on the Thesis including bi-weekly meeting out of his busy schedule. He is my primary resource for getting my thesis questions answered and was instrumental in helping me crank out this thesis. I would have been lost without him.

### **Thesis Committee (Inside Member) – Dr. Michael Santora**

I would also like to express my gratitude to my inside member Dr. Michael Santora for his willingness to be part of my committee.

**Technical Advisor – Dr. Sorin Deleanu**

I would like to take this opportunity to thank Dr. Deleanu for his assistance and actively participation. This thesis would not have been possible without the help, support and patience of him, not to mention his advice and unsurpassed knowledge of the machine and motor drive expertise. I greatly appreciate him taking the time to answer my question, his high quality of works, and his many suggestions concerning topics, new directions and sharing of his technical expertise in power electronic technology, electric machines and motor drive application. With his help, I was able to understanding of concepts of DTC and be able to apply it in this thesis. I would like to special thanks to his professional engineering mentorship for last 10 years.

**Technical Advisor - Rammohan Nandiraju**

He is my best colleague while I was working at AltaSteel. I am using this special opportunity to express my gratitude to Rammohan for sharing his truthful and illuminating views on a number of technical issues related to the research project. I am also very grateful for his mechanical engineering advice, knowledge, insightful discussions and suggestions regarding about the thesis. During the conceptual stage of this research project, he provides me an aspiring guidance, constructive criticism and friendly advices which are proven invaluable for the thesis development stage.

**Colleague – Dr. JP Provost**

I am indebted to Dr. Provost, my colleague at NAIT with his enthusiasm, inspiration on the topic. Throughout my thesis-writing period, he provided encouragement, sound advice to me and lots of stimulating discussion among us.

**AltaSteel Ltd.**

I would like to express my gratitude to AltaSteel Ltd. AltaSteel gave me a chance to growth professionally for 11 years from Electrical Technologist in training to Advanced Electrical Drives Engineer. I owe a debt of gratitude to AltaSteel to allow me to works on different automation and drives projects like Roughing Mill DC drives; Reheat Furnace Upgrade; Finishing Mill ABB Drives; Bundling Siemens Drives Upgrade and etc. I am truly grateful that AltaSteel allowed me to work on this exciting Crop Cobble Shear operation improvement project. Besides, it also provides all necessary resources (equipments, information, time and finance). This thesis would not have been possible without support from AltaSteel.

**The Northern Alberta of Institute of Technology (NAIT)**

I would like to acknowledge the financial, academic and technical support of NAIT, Edmonton, Alberta and its staff, particularly in the award of a credential enhancement fund that provided the necessary financial support for this thesis.

## **Dedication**

This Thesis is dedicated to my father, my wife and my two lovely sons.

For their endless love, support and encouragement.

## Table of Contents

Authorization to Submit Thesis .....	ii
Abstract .....	iii
Acknowledgements .....	iv
Dedication .....	vii
Table of Contents .....	viii
List of Figures .....	x
List of Tables .....	xii
Notations .....	xiii
Chapter 1: Introduction .....	1
1.1 Purpose .....	1
1.2 Background .....	1
1.3 Scope and Methodology .....	3
Chapter 2: Literature Search .....	5
Chapter 3: DTC System Overview .....	9
3.1 Overview and Background .....	9
3.2 DTC Classical Control Strategy .....	12
3.2.1 Induction Motor Torque Production .....	12
3.2.2 Torque Controller and Flux Controller .....	13
3.2.3 Optimum Pulse Selector .....	14
3.2.4 Adaptive Motor model .....	22



3.3 Matlab/SimPowerSystems Simulations .....	24
3.3.1 SimPowerSystems DTC Motor Drive Block .....	24
3.3.2 Induction Motor Dynamic Model used in Simulation .....	27
Chapter 4: Problem Definition, Solution and Simulations .....	30
4.1 Problem Definition .....	30
4.2 Solution and Simulations .....	36
Chapter 5: System Design .....	38
5.1 CCS System Overview .....	38
5.2 SBL Programming .....	39
5.2.1 Introduction to SBL .....	39
5.2.2 CCS SAFphire Modeling .....	40
5.2.3 SBL Program Modification .....	42
Chapter 6: Results from the Physical System .....	46
Chapter 7: Conclusion and Future Recommendation .....	47
7.1 Conclusion .....	47
7.2 Future Recommendation .....	48
References .....	49
Appendices .....	52
A. Project Pictures .....	52
B. ABB ACS600 Drives Model, Parameters and Ratings .....	54
C. Motor Information .....	56

## List of Figures

Figure 1: Crop Cobble Shear .....	1
Figure 2: CCS Cascade Control Loop .....	2
Figure 3: Basic Direct Torque Control Block Diagram .....	10
Figure 4: DTC Torque Control Loop Block Diagram .....	13
Figure 5: Stator Flux Vector and Sectors .....	14
Figure 6: Inverter Voltage Vectors .....	15
Figure 7: Inverter and Induction Motor Schematic Diagram .....	17
Figure 8: Inverter and Induction Motor with Switching State .....	17
Figure 9: Eight Possible Switching States .....	18
Figure 10: Stator Flux Vector Trajectory.....	19
Figure 11: SimPowerSystems DTC Block Diagram .....	24
Figure 12: Overview of DTC Control Block .....	25
Figure 13: DTC Controller Block Diagram .....	25
Figure 14: Real World System Result (Pre-Modification) .....	30
Figure 15: Simulation Model .....	31
Figure 16: Induction Motor Parameters.....	33
Figure 17: Simulation Result (Pre-Modification) .....	34
Figure 18: Output Current Overload Characteristic Graph .....	35
Figure 19: DTC Drive 200% Duty Cycle .....	35
Figure 20: Simulation Result (Post-Modification) .....	37
Figure 21: CCS DTC Control Block Diagram .....	38
Figure 22: CCS SAFphire System .....	39

Figure 23: SAFphire SBL Software .....	40
Figure 24: CCS Front View .....	40
Figure 25: CCS Blade Position .....	41
Figure 26: CCS Speed Controller Output .....	43
Figure 27: CCS Speed Controller .....	43
Figure 28: CCS Speed Reference .....	44
Figure 29: CCS Lock Speed Logic (Pre-Modification) .....	45
Figure 30: CCS Lock Speed Logic (Post-Modification) .....	45
Figure 31: Real World Result (Post-Modification) .....	46
Figure 32: Rolling Mill Electrician during Commissioning .....	52
Figure 33: Rolling Mill Operator during Commissioning .....	52
Figure 34: ABB CCS DTC Drive .....	53

## List of Tables

Table 1: Voltage Space Vector and Binary Definition .....	16
Table 2: Inverter Voltage Vectors Switching Table .....	21
Table 3: Example for Torque and Flux Variation .....	21
Table 4: CCS Drive Parameters .....	54
Table 5: ABB ACS600 Drive Rating .....	55
Table 6: CCS ABB Motor Information .....	56

## Notations

$T_e$  Electromagnetic Torque

$i_s$  Stator Current

$i_{qs}$  q-axis stator current in arbitrary reference frame

$i_{ds}$  d-axis stator current in arbitrary reference frame

$i_{qs}^s$  q-axis stator current in stationary reference frame

$i_{ds}^s$  d-axis stator current in stationary reference frame

$i_{qr}$  q-axis rotor current in arbitrary reference frame

$i_{dr}$  d-axis rotor current in arbitrary reference frame

$i_{qr}^s$  q-axis rotor current in stationary reference frame

$i_{dr}^s$  d-axis rotor current in stationary reference frame

$v_{qs}$  q-axis stator voltage in arbitrary reference frame

$v_{ds}$  d-axis stator voltage in arbitrary reference frame

$v_{qs}^s$  q-axis stator voltage in stationary reference frame

$v_{ds}^s$  d-axis stator voltage in stationary reference frame

$\psi_{qs}$  q-axis stator flux in arbitrary reference frame

$\psi_{ds}$  d-axis stator flux in arbitrary reference frame

$\psi_{qs}^s$  q-axis stator flux in stationary reference frame

$\psi_{ds}^s$  d-axis stator flux in stationary reference frame

$\alpha$  angle between stator flux and stator current

$\gamma$  angle between stator flux and rotor flux

$T_{ref}^*$  Torque Reference

$T_{act}$  Actual Torque Feedback

$T_{err}$  Torque Error

$\psi_s^*$  Stator Flux Reference

$\psi_{act}$  Actual Stator Flux Feedback

$\psi_{err}$  Stator Flux Feedback

$H_T$  Torque Loop Controller Three Level Digital Output

$H_\psi$  Flux Loop Controller Two Level Digital Output

$S_A$  Inverter Output A Output Signal

$S_B$  Inverter Output B Output Signal

$S_C$  Inverter Output C Output Signal

$s(k)$  Stator Flux Position (in Sector)

SCIM Squirrel Cage induction Motor

DTC Direct Torque Control

FOC Field Oriented Control

CCS Crop Cobble Shear

VFD Variable Frequency Drive

SBL SAF Block Language

## Chapter 1: Introduction

### 1.1 Purpose

The purpose of the thesis is to investigate how to identify the root cause of the CCS overcurrent issue. Through the simulation and design process, identifies the proper method to modify the existing DTC induction motor drive control system in order to improve the performance of the CCS.

### 1.2 Background



Figure 1: Crop Cobble Shear

A Crop Cobble Shear (CCS) is a system for cutting steel bar and is used in a steel rolling mill (Figure 1). In normal operation, the CCS performs a single cut to chop each end of the bar. One of the alternative but significant functions of the CCS occurs when cobble is required. In this mode, the shear will chop the bar into small lengths. This operation is known as cobble cutting mode (continuous cutting).

In normal cutting mode, accurately cutting the bar to a specific length is crucial. This means that high performance control is required. The CCS control consists of three control loops (Figure 2) and they are from outer to inner: Position Loop – Speed Loop – Torque Loop [28].

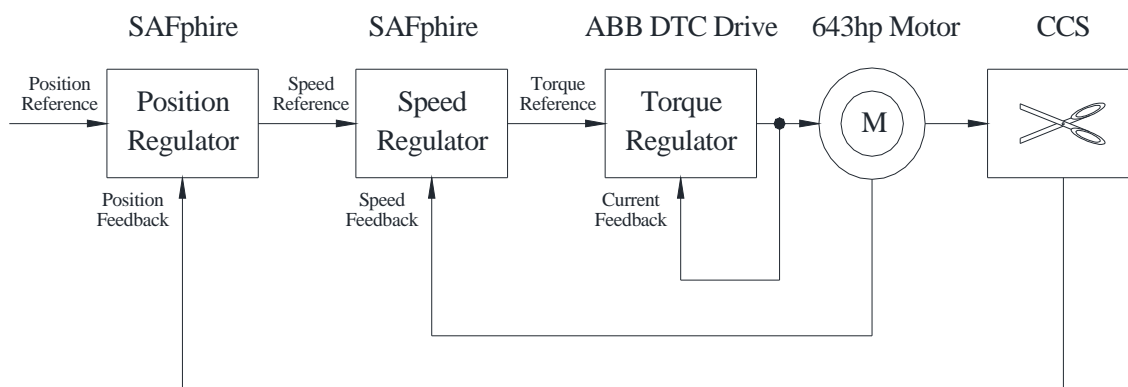


Figure 2: CCS Cascade Control Loop

The overall objective of the CCS is to accurately cut the head or tail end of the bar during normal rolling. In order to achieve accurate cut length, continuous position control of the blade is required (the outer loop of Figure 2). The output of the position loop is the speed reference required to correct the position error. This speed reference is fed into the intermediate speed loop. The responsibility of the speed loop is trying to eliminate the speed error of the motor. The output of the speed loop is torque reference which also changes continuously and dynamically in order to achieve zero speed error. Since all three control quantities are constantly changing, therefore, CCS control loop is classified as a highly dynamic application.

Since CCS is a highly dynamic control application, therefore, the Direct Torque Control (DTC) drive is used. DTC was introduced in the 1980's and adopted by industry more readily than vector control [1]-[4]. DTC is a significantly newer concept compared to



Field Oriented Control (FOC); DTC is the most advanced AC drive technology in the world [26]. DTC uses the fastest digital signal processing hardware available and an advanced mathematical model of an induction motor, the result is high dynamic performance and fast torque response [26]. In addition, it provides very fast, accurate, reliable flux control. DTC provides very fast response with a simple control structure compare to FOC, DTC control is gaining popularity in industries more rapidly than FOC [1]-[4].

However, during the cobble cutting mode, depending on the bar length, it has been observed that the DTC drive frequently experiences overcurrent faults that creates a fault condition in the drive. If the drive fault occurs during cobble cutting, the faults and other repercussions may be serious and dangerous. It could potentially damage other equipment and create safety concerns. In order to develop an improvement to the operation of the CCS and to avoid the overcurrent fault issue, the DTC motor drive system was simulated based on the information available for the motor. A potential solution was identified that would reduce or eliminate the overcurrent faults. The modified system was again simulated to show how the improvement would impact the operations. Finally this solution was implemented on the production system and the result shows that the modified method of CCS operation is very successful.

### **1.3 Scope and Methodology**

This research project is focused on how to improve the operation of the CCS DTC control to resolve the overcurrent issue. The scope of the research project includes the following steps:

1. Gathering data includes the field measurements of CCS real time operation information, CCS motor parameters, CCS DTC drive technical specifications CCS system control system configurations
2. Full analysis of the information and data in order to identify the root cause of overcurrent
3. Perform simulations of the existing DTC induction motor drive system
4. Propose solution to reduce or eliminate the overcurrent faults
5. Perform simulations that include the proposed solution to predict the result and impacts on the original system
6. Perform design of the real world modification
7. Perform the real world modification to record the result
8. Test the modified system to determine if the proposed solution resulted in a suitable solution to the fault problems
9. Document the results and methods

In addition to the technical textbooks and manuals listed in the references section, information is gathered through a literature search to gain an in-depth understand how the DTC induction motor drive system is applied to high dynamic control application. A summary of the important points of this literature search is found in Chapter 2.

## Chapter 2 – Literature Search

In the past, Direct Current (DC) machines were used extensively for variable speed applications. The reason is because DC machine's armature and field current can be control separately and hence, the torque and flux of the machine can also be controlled independently. However, the major drawback of using DC motor is the presence of commutator and brush assembly, which causing very high maintenance cost, limited speed range and applications. Therefore DC motors have started to be replaced by more advanced motor technology in industrial applications.

Due to the robustness, low cost of maintenance and rapid evolution of power electronics, the Squirrel Cage Induction Motor (SCIM) has become very popular in industrial motor variable speed drive application. Induction motors are widely used and are the most common motor in many industries [5]. When designing an electrical motor drive system, the motor usually is the starting point [10]. In modern AC motor drive controls, there are two types of drives employed for high performance applications: DTC and FOC [14]. In the FOC control strategy, the operation of the induction motor can be analyzed mathematically in a similar way to a DC motor. In contrast, DTC makes direct use of physical interactions that take place between the motor and supply. Therefore, the co-ordinate transformation and intermediate current loop are not required. This means that the torque is controlled directly [1]. The DTC scheme provides excellent speed and torque regulation without speed feedback [26]. The electromagnetic torque and stator flux magnitude are estimated with stator voltages and currents; therefore with the exception of stator resistance, motor parameter variations do not affect the estimation.

There are many papers and textbooks published regarding DTC induction motor drives theory and background [1]-[4], [10]-[14], [22]-[25], [36]. Researchers focus on methods to improve DTC performance such as how to reduce torque ripple [11]; using space vector modulation to improve the DTC performance [13]; comparison studies between DTC and FOC [10]. In general, research suggests the following key points regarding DTC [10]-[14], [22]-[25]:

- DTC is one of the best control methods for motor drives
- It allows decoupled control of motor stator flux and electromagnetic torque
- By selecting the appropriate voltage vector, high torque response can be obtained
- DTC needs stator flux and torque estimation; therefore it is not sensitive to rotor parameters
- DTC is inherently a motion-sensorless control method

Because of the maturity of DTC theory, this thesis only presents the classical DTC control in Chapter 3. Then it focuses on how to improve the CCS DTC induction motor drive operation to resolve the overcurrent issue by using a practical engineering approach.

Due to the uniqueness of the system and specific applications within the company, there is very limited CCS information available. There is neither documentation nor institutional resources that indicate the existence of a specific solution to this CCS overcurrent problem. During the literature search, it is apparent that CCS is a highly dynamic load and a high performance AC drive such as DTC is required [15]-[21].

There are many industrial electromechanical systems requiring precisely control torque, speed, and position [2], [27]. The steel rolling mill is a highly demanding application for a motor drive system. High performance drives are always preferable for the main rolling

mill stands and shears equipment [15]-[21]. More demanding drive applications used in rolling mills have much more sophisticated requirements and must be able to handle the dynamic requirements to allow for controlling of a number of variables, such as speed, position, acceleration, and torque. Such high-performance applications typically require excellent steady state and dynamic performance as well as a wide speed range and fast transient response [26].

The main functions of CCS are to provide front end and tail end cut during normal operation [16]. This function “crops” the unwanted poor quality sections of the bar that are usually located at the beginning and end. By removing these sections the quality of the rolling is enhanced. Another function of the CCS is if an unexpected event happens which cause the bars cobble, then the CCS performs a continuous cutting (cobble cutting) such that the bar will be cut in smaller pieces. Cobble is an incident when bar that is being hot rolled either jams in the entry of the mill stand, or comes out of its normal rolling path. In this case, the rolling process has to stop. The cobble cutting function of CCS can help for bar handling and prevent equipment damage. The speed at which a shear is able to cut the steel bar is dependent upon many variables including:

- the rotating speeds of the shear
- the shear blade conditions
- the grade and mass of the steel bar
- the steel temperature
- the linear speed of the bar at shearing

It may cause compression, or mill push into the bar, if the shear cut is too slow relative to the bar linear speed. This may cause the bar to buckle against the back of the shear blade. The

bar may even cobble at the shear to certain extreme cases. On the other hand, if the shear cut is too fast relative to the bar linear speed, the shear's blade may impact with the tail of the bar ("kick" the bar). This impact could cause a bend in the tail of the bar. This deformation result in reduced quality or damage due to impact with equipment. Due to the above reasons, the CCS position, torque and speed control is crucial for the success of the system [15]-[21]. Therefore, a high performance torque control drive is required. If the drive control system is not tuned to operate at optimal performance, the drive fault is resulted.

In summary, because CCS is the complex and highly dynamic application, a high performance drive control is required and DTC is well suited for this application.

## Chapter 3 – DTC System Overview

### 3.1 Overview and Background

When machine control techniques are considered for a specific application. There are a number of approaches that can be taken. Some of the more common approaches are FOC, Vector Control and Direct Torque Control (DTC).

Unlike FOC or vector control techniques, in the DTC scheme, there is no dq-axis transformation needed. The electromagnetic torque and the stator flux are estimated or calculated and directly controlled by applying the appropriate stator voltage vector through the optimum pulse selector [2].

This control strategy makes use of the physical interactions between the drive and machine, such that it can directly control the torque and stator flux of a machine. This is achieved by applying inverter voltage space vector selection through a lookup table. The DTC control unit is composed of two parallel closed loops; one for the stator flux and one for the torque [1]-[4]. The torque reference can be imposed directly if the control unit operates in torque mode. Alternatively, the torque reference can be delivered at the output of the speed controller if the DTC operates in speed mode. According to earlier work [1]-[4], this type of control system shows significant differences when compared to vector control. These differences are:

- no coordinate transformation is required and the induction motor system is modeled in the stator reference frame;
- direct control of the flux and torque;
- instead of knowing the exact position of stator flux linkage space vector, only the sector containing the stator flux linkage space vector is required;

- current controllers are not required;
- since speed information is never required in the torque mode of operation, DTC is inherently sensorless;
- does not require a separate voltage modulation block. This is usually required in vector drive;
- minimum switching frequency.

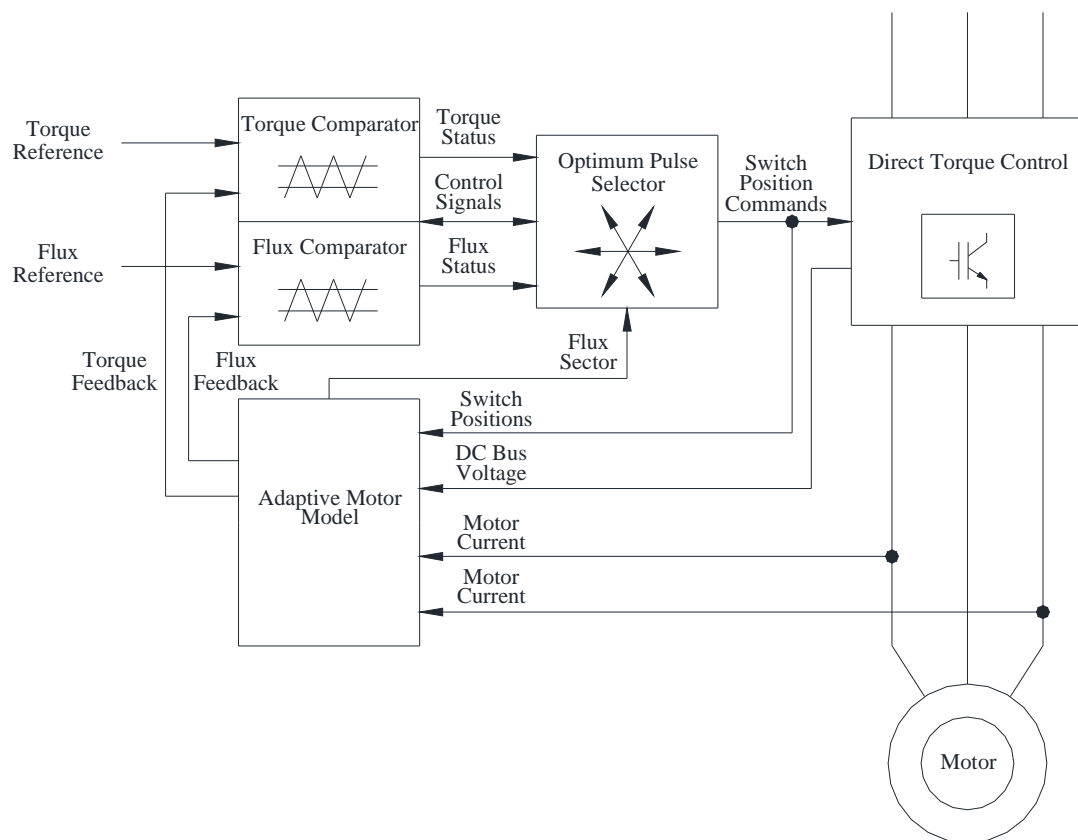


Figure 3: Basic Direct Torque Control Block Diagram

The DTC Block diagram is shown in Figure 3 and since the CCS DTC drive is programmed in torque control mode, the torque reference comes from an external high level speed controller. The speed controller is based on a PI regulator and the output is a torque set point applied to the DTC controller block. The adaptive motor model estimates the motor



torque and stator flux with feedback to the torque and flux comparators. This allows for the torque and flux control loop to be established [1]-[4]. The torque comparator is a three-level hysteresis controller and the flux comparator is two-level hysteresis controller. The switching output of inverter depends on the torque status signals and flux status signals from torque and flux comparator. Using torque and flux status signals, along with the knowledge of the calculated position feedback of the stator flux linkage space vector from the adaptive motor model, an appropriate voltage vector is selected inside the optimum pulses selector. Note that when compared to a vector control drive, the error between torque/flux setpoints and feedbacks in DTC are used in a different way. The outputs of the controller are the d-q axis current setpoints to the current controllers. However, DTC applies the error signals directly to the optimum pulse selector to control the inverter without any intermediate current control loops or co-ordinate transformation.

## 3.2 DTC Classical Control Strategy

### 3.2.1 Induction Machines Torque Production

The torque equation of induction motor can be expressed in terms of stator flux / rotor flux: [1]-[4]

$$T_e = \frac{3}{2} \frac{P}{2} \frac{L_m}{\sigma L_s L_r} |\psi_r| |\psi_s| \sin \gamma. \quad (3.1)$$

The change of rotor flux is slow due to its relatively large rotor time constant. This means that the rotor flux may be approximated to a constant for a short period of time. Also, the stator flux amplitude is kept constant in a DTC scheme by using the two level hysteresis controller. If instantaneous positions of the stator flux space vector are changed rapidly such that angle  $\gamma$  is also changed rapidly, the rapid rate of change of torque can be obtained and fast torque response results. This is the core concept of DTC. The instantaneous torque can be expressed in terms of the stator current and the stator flux as follow:

$$T_e = \frac{3}{2} \frac{P}{2} |\psi_s| |i_s| \sin \alpha. \quad (3.2)$$

If the stator flux is kept constant, then the output torque depends on the magnitude of stator current and the position between stator flux/stator current space vectors. Therefore, in general, if the output torque demand is higher, the motor will draw higher current. If the stator resistance of the motor is neglected, the stator flux equation can be written as follow:

$$V_s = \frac{d}{dt} (\psi_s) \quad (3.3)$$

$$\Delta \psi_s = V_s \Delta t. \quad (3.4)$$

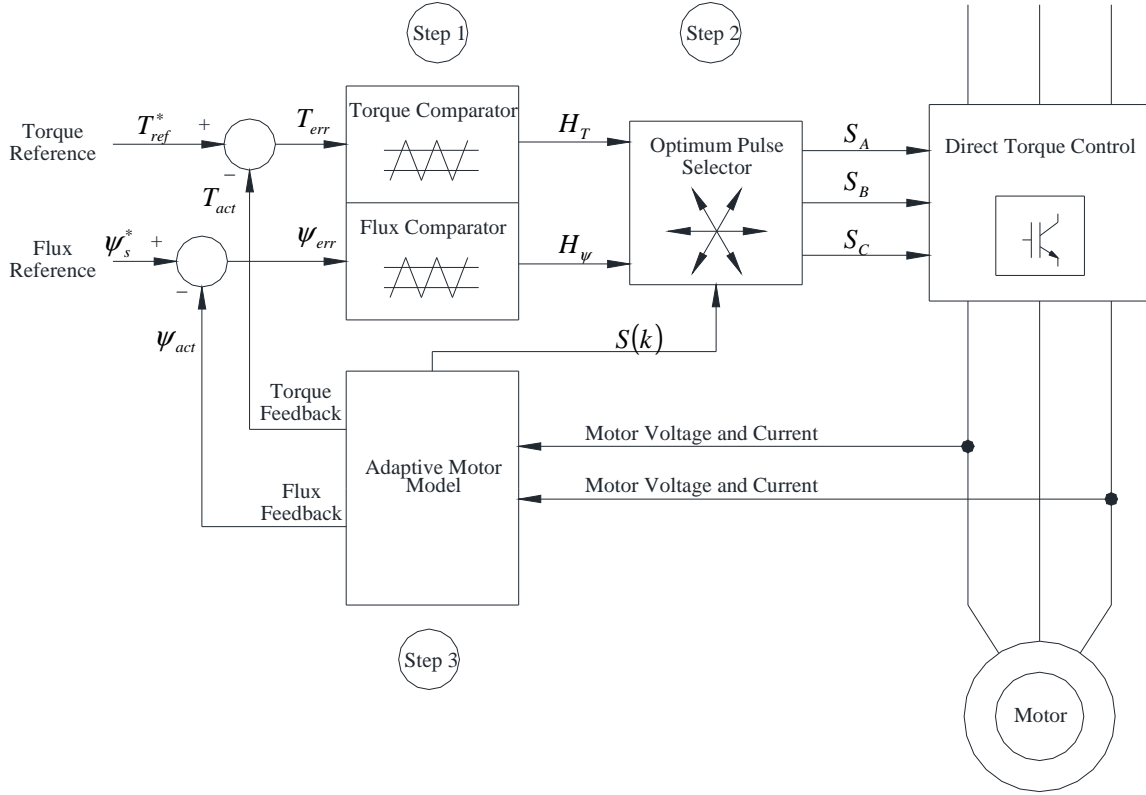


Figure 4: DTC Torque Control Loop Block Diagram

### 3.2.2 Torque Controller and Flux Controller

Referring to Figure 4 Step 1, the function of the torque/flux loop control is to control the torque/flux error, which resulted in the difference between torque/flux reference and torque/flux feedback, within a preset bandwidth which is called the hysteresis band width [3], [26]. The torque reference  $T_{ref}^*$  and stator flux reference  $\psi_s^*$  are compared with the respective estimated values, that are calculated by the flux estimator inside the adaptive motor model, and the result is torque error  $T_{err}$  and flux error  $\psi_{err}$ . The errors are fed into 3-level torque loop controller and 2-level flux loop controller which are hysteresis band type controllers, where  $2HB_\psi$  is the total hysteresis band width of the flux loop controller.

The stator flux reference space vector is shown in Figure 5 and it rotates in an anti-clockwise direction. The actual stator flux is controlled within the hysteresis band by Flux loop controller.

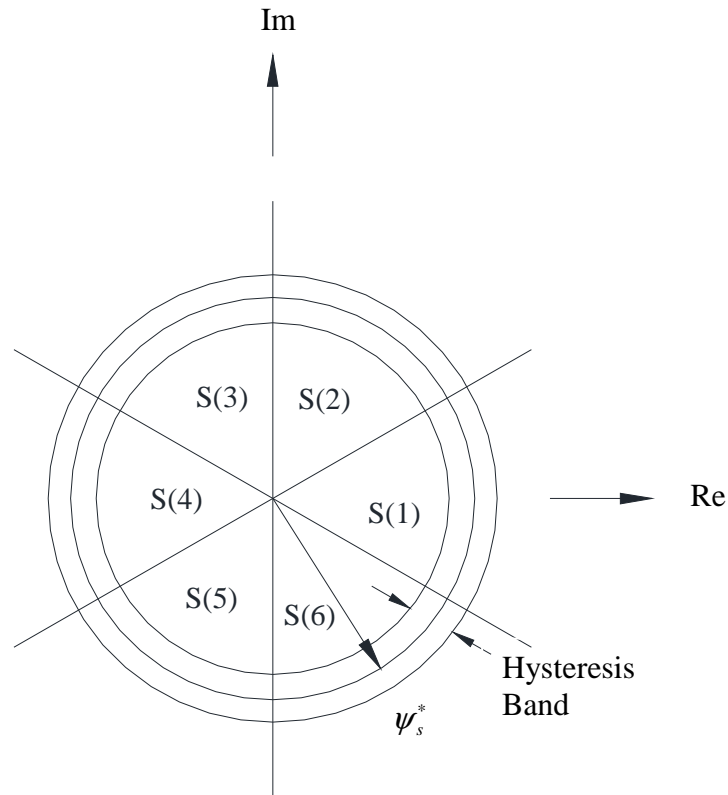


Figure 5: Stator Flux Vector and Sectors

### 3.2.3 Optimum Pulse Selector

The optimum pulse selector (also called inverter switching table or voltage vector table) is shown in Figure 4 Step 2. It is a digital signal processor (DSP), together with ASIC hardware that determines the switching logic of the inverter [26]. This configuration provides the inverter's semiconductor switching devices with an optimum switching frequency for the motor torque. There is no fixed switching pattern as is found in traditional PWM and the switching pattern is determined by demand. DTC is also known as “just-in-time” switching,

and every switching is necessary and used. After the optimum pulse selector receives the input signals  $T_{err}$ ,  $\psi_{err}$  and the flux position in term of sectors  $S(k)$ , then it generates the appropriate control voltage vector (switching states) for the inverter from a lookup table. The sections of the plane for stator flux are all 60 degrees (Figure 6).

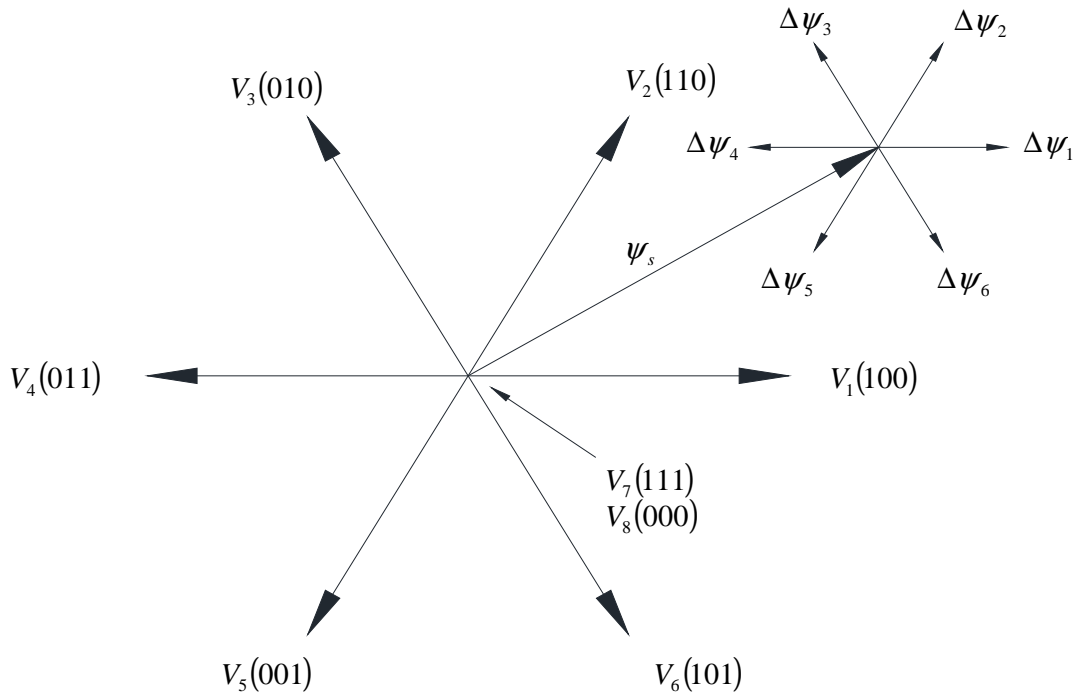


Figure 6: Inverter Voltage Vectors

If the stator flux space vector lies in the  $k$ th sector, where  $k=1, 2, 3, 4, 5$  or  $6$ , the flux magnitude is increased by using  $K+1, K-1$ . Conversely, the flux magnitudes is decreased by using  $K+2, K-2$  and  $K+3$  vectors. In other words, by applying either the voltage vector belonging to the sector or any of the two voltages vectors beside it, the stator flux value will be increased. Not only the stator flux, however, the induction motor's torque magnitudes and the switching frequencies are all affected by the applied voltage vector. Therefore, the overall

concept is to try to select the most appropriate voltage space vector such that the following three objectives are achieved

1. keep the switching frequency as low as possible (just-in-time concept) requires the minimum amount of switching;
2. control the stator flux errors with the hysteresis band width;
3. control torque errors within the hysteresis band width.

From Table 1, the definition of inverter switching states are clearly defined in terms of a set of binary signals. There are six non-zero voltage space vectors  $V_1, V_2, V_3, V_4, V_5, V_6$  and two zero voltage space vectors  $V_7$  and  $V_8$ . Figure 7, 8, 9 are the circuit diagrams for inverter switching states. For each of the six possible non-zero space vectors, change from one to the other is only required switching one inverter leg. For example, if the inverter operation requires switching from  $V_1 = 100$  to the next voltage vector, then subsequent vectors are either  $V_2 = 110$ ,  $V_6 = 101$  or  $V_8 = 000$ . Minimum or just-in-time switching frequency is achieved in this way. The torque loop controller and flux loop controller will determine which of the three possible vectors will be applied depends on the flux and torque errors.

Voltage Space Vector	Binary Definition
$V_1$	100
$V_2$	110
$V_3$	010
$V_4$	011
$V_5$	001
$V_6$	101
$V_7$	111
$V_8$	000

Table 1: Voltage Space Vector and Binary Definition

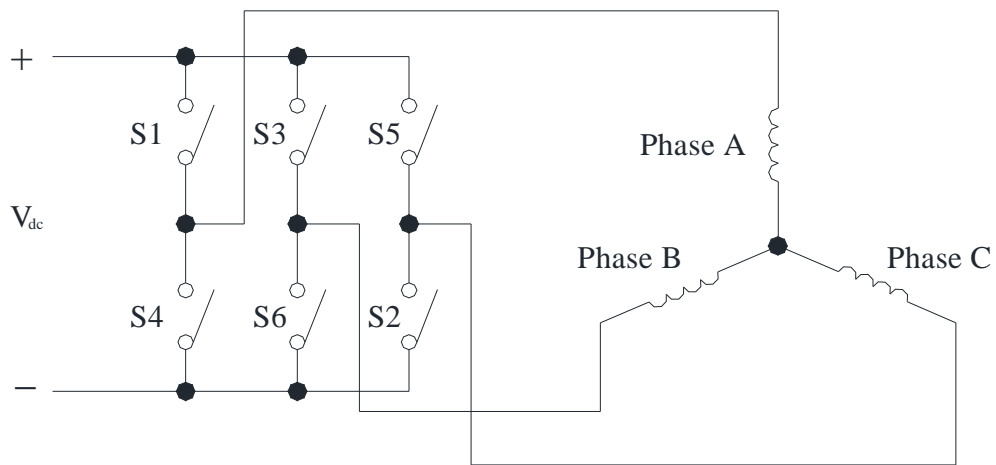


Figure 7: Inverter and Induction Motor Schematic Diagram [4]

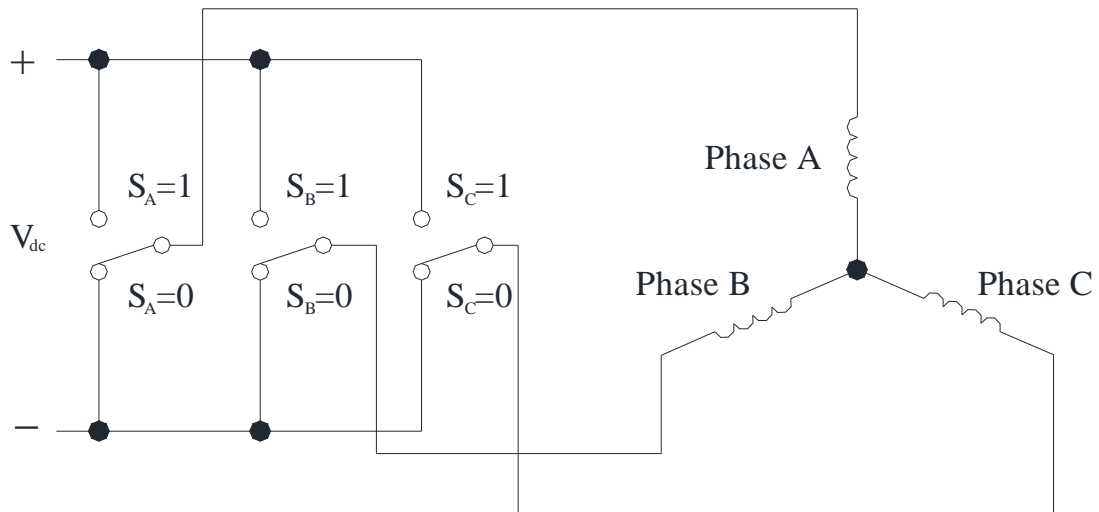


Figure 8: Inverter and Induction Motor with Switching State [4]



Figure 9: Eight Possible Switching States [4]



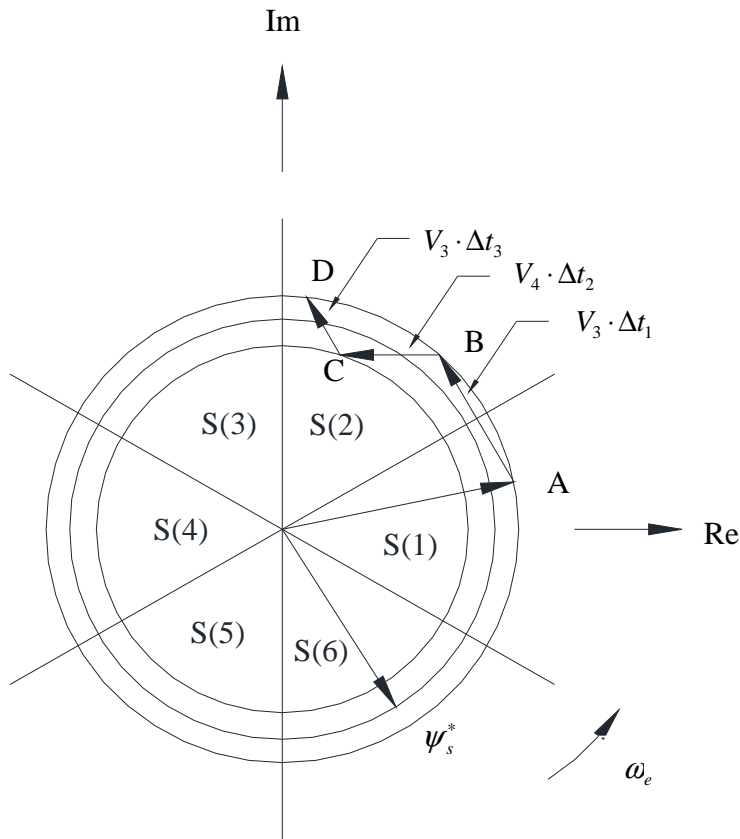


Figure 10: Stator Flux Vector Trajectory [3]

A sample switching operation will be illustrated in Figure 10. Assume the DTC drive is operated below the base speed of the motor such that the stator flux reference is constant and equal to rated stator flux. The actual stator flux direction rotates in anti-clockwise direction and is only allowed to vary between a hysteresis bandwidth. It is assumed that at certain times, the stator flux is located in sector 1 and reaches the outside boundary of the hysteresis band (Point A). In order to reduce the stator flux magnitude, a different voltage space vector has to be applied. Referring to Table 1, if voltage vectors 1, 2 or 6 apply to the motor terminals, the stator flux is increased. If voltage vectors 3, 4 or 5, reduction in stator flux magnitude is resulted. Out of the three vectors, vector 3 requires switching only one of

the inverter legs. Therefore, Vector 3 is applied to the motor terminals and controls the stator flux path toward to point B.

At Point B, the stator flux needs to reduce because it reaches the outer boundary again, the possible voltage vectors that will result the reduction of the stator flux are vectors 4, 5 or 6. In this case, Vector 4 is the one requires switching in only single inverter leg. Therefore, voltage vector 4 is applied to the motor terminals and controls the stator flux towards the inner boundary of the hysteresis band (Point C).

At point C, the stator flux needs to increase because it reaches the inner boundary. The possible voltage vectors that will result in increase the magnitude of stator flux are vectors 1, 2 or 3. Voltage vector 3 is the one that requires switching in only a single inverter leg. Therefore, voltage vector 3 is applied to the motor terminals and controls the stator flux towards the outer boundary of the hysteresis band (Point D) and the process continues.

So far, only two objectives of DTC control states have been achieved as shown on Page 16. The selection of the voltage space vector has to consider torque error as well. There are three conditions for controlling the torque error:

1. Stopping the rotation of stator flux space vector. the torque magnitude will stay unchanged
2. Stator flux vector rotated to a forward position. This will generate a positive torque
3. Stator flux vector rotated to a backward position. This will generate a negative torque.

The flux loop controller has the following relations:

If  $\psi_{err} > +HB_{\psi}$ , then  $H_{\psi} = 1$

If  $\psi_{err} < -HB_{\psi}$ , then  $H_{\psi} = -1$

The torque control loop has the following relations:

If  $T_{err} > +HB_T$ , then  $H_T = 1$

If  $T_{err} < -HB_T$ , then  $H_T = -1$

If  $-HB_T < T_{err} < +HB_T$ , then  $H_T = 0$

And the operations to meet all three objectives are summarized in Table 2

$H_{\psi}$	$H_T$	Sector 1	Sector 2	Sector 3	Sector 4	Sector 5	Sector 6
1	1	$V_2$	$V_3$	$V_4$	$V_5$	$V_6$	$V_1$
1	0	$V_8$	$V_7$	$V_8$	$V_7$	$V_8$	$V_7$
1	-1	$V_6$	$V_1$	$V_2$	$V_3$	$V_4$	$V_5$
-1	1	$V_3$	$V_4$	$V_5$	$V_6$	$V_1$	$V_2$
-1	0	$V_7$	$V_8$	$V_7$	$V_8$	$V_7$	$V_8$
-1	-1	$V_5$	$V_6$	$V_1$	$V_2$	$V_3$	$V_4$

Table 2: Inverter Voltage Vectors Switching Table

An example for flux and torque change for applying voltage vectors for the location of  $\psi_s$  is shown in Table 3 and Figure 6.

Voltage Vector	$V_1$	$V_2$	$V_3$	$V_4$	$V_5$	$V_6$	$V_7$	$V_8$
$\psi_s$	+	+	-	-	-	+	0	0
$T_e$	-	+	+	+	-	-	-	-

Table 3: Example for Torque and Flux Variation due to Apply Voltage Vectors

### 3.2.4: Adaptive Motor Model

Referring to Figure 4 Step 3, the measured information from the motor, including stator voltages and currents, are fed to the Adaptive Motor Model (also called the Flux Estimator). The adaptive motor model is essentially a flux estimator that is used to calculate the torque feedback and the flux feedback that feeds into the torque and flux comparators respectively. In addition, the flux estimator can also provide the stator flux space vector position in terms of sector that feed to the optimum pulse selector. Before the DTC drive is put into operation, the actual motor parameters are fed into the DTC drive and this process is known as the motor identification run. Stator resistance, mutual inductance and the motor's inertia are extracted during the auto-tuning process [28]. After the motor model is established, then the flux estimator is ready to perform the calculations as described below. Classical DTC control is modeled with a stationary reference frame and using dq modeling [1], the first step is performing a three-to-two phase transformation shown in Eq. (3.5)-(3.7).

$$\begin{bmatrix} i_{qs}^s \\ i_{ds}^s \\ i_o^s \end{bmatrix} = \frac{2}{3} \begin{bmatrix} 1 & -\frac{1}{2} & -\frac{1}{2} \\ 0 & -\frac{\sqrt{3}}{2} & \frac{\sqrt{3}}{2} \\ \frac{1}{2} & \frac{1}{2} & \frac{1}{2} \end{bmatrix} \begin{bmatrix} i_a \\ i_b \\ i_c \end{bmatrix} \quad (3.5)$$

$$i_{qs}^s = \frac{2}{3}i_a + \frac{1}{2}(i_b + i_c) = i_a \quad (3.6)$$

$$i_{ds}^s = -\frac{1}{\sqrt{3}}i_b + \frac{1}{\sqrt{3}}i_c \quad (3.7)$$

The stator voltage is then calculated with Eq. (3.8), (3.9) and (3.10).

$$\begin{bmatrix} v_{qs}^s \\ v_{ds}^s \\ v_o \end{bmatrix} = \frac{2}{3} \begin{bmatrix} 1 & -\frac{1}{2} & -\frac{1}{2} \\ 0 & -\frac{\sqrt{3}}{2} & \frac{\sqrt{3}}{2} \\ \frac{1}{2} & \frac{1}{2} & \frac{1}{2} \end{bmatrix} \begin{bmatrix} v_{an} \\ v_{bn} \\ v_{cn} \end{bmatrix} \quad (3.8)$$

$$v_{qs}^s = \frac{2}{3} v_{an} - \frac{1}{3} v_{bn} - \frac{1}{3} v_{cn} \quad (3.9)$$

$$v_{ds}^s = -\frac{1}{\sqrt{3}} v_{bn} - \frac{1}{\sqrt{3}} v_{cn} \quad (3.10)$$

After stators voltages and currents are obtained in the dq model and stationary reference frame, the stator flux can be calculated with Eq. (3.11), (3.12) and (3.13).

$$\psi_{ds}^s = \int (v_{ds}^s - r_s i_{ds}^s) dt \quad (3.11)$$

$$\psi_{qs}^s = \int (v_{qs}^s - r_s i_{qs}^s) dt \quad (3.12)$$

$$|\psi_s^s| = \sqrt{(\psi_{ds}^s)^2 + (\psi_{qs}^s)^2} \quad (3.13)$$

The last step is calculating the developed torque with Eq. (3.14).

$$T_e = \frac{3P}{2} (\psi_{ds}^s i_{qs}^s - \psi_{qs}^s i_{ds}^s) \quad (3.14)$$

### 3.3 Matlab/SimPowerSystems Simulations

#### 3.3.1 SimPowerSystems DTC Induction Motor Drive Block

The SimPowerSystems DTC Induction Motor Drive block (Figure 11) is built from six main blocks [9].

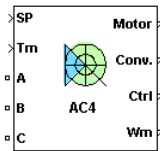


Figure 11: SimPowerSystems DTC Block [9]

The high-level schematic shown in Figure 12 is built from six main blocks including:

1. Three Phase Diode Rectifier
2. Three Phase Inverter
3. Speed Controller
4. Braking Chopper
5. DTC
6. Induction Machines

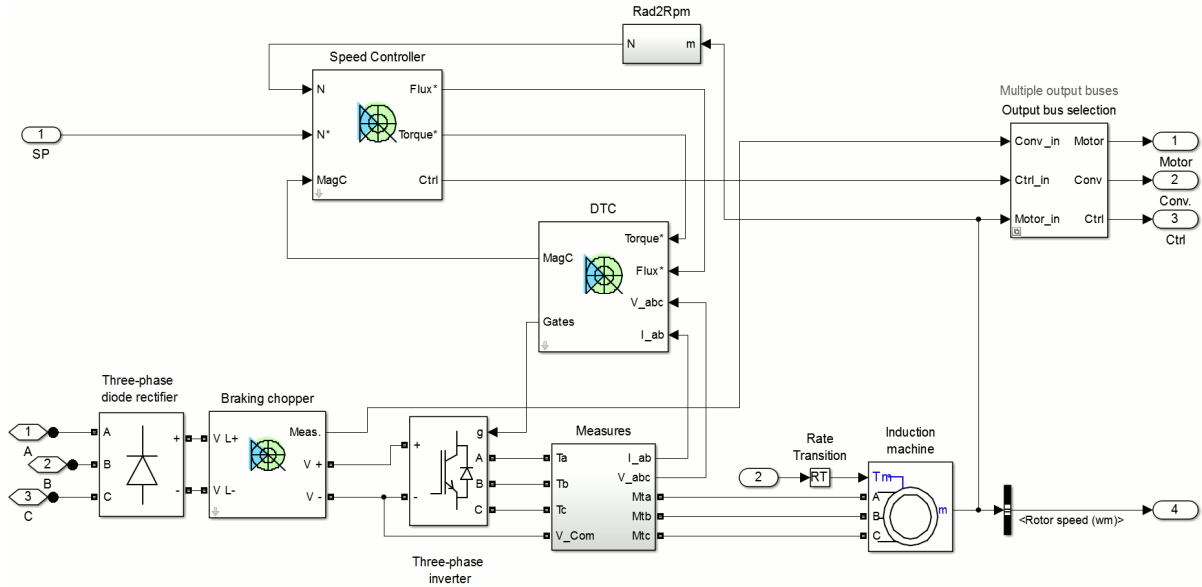


Figure 12: Overview of DTC Control Block [9]

Within the DTC controller, it has five main blocks and they are Torque & Flux calculator,  $\alpha\beta$  vector, Torque and Flux hysteresis, Switching table and switching control (shown in Figure 13).

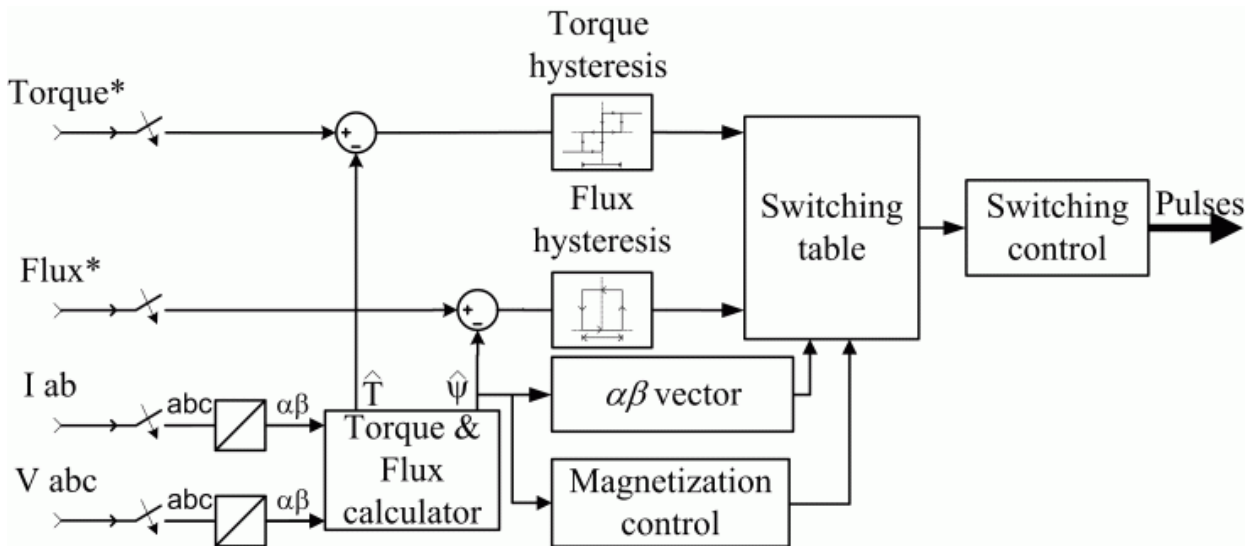


Figure 13: DTC Controller Block Diagram [9]

The Torque & Flux calculator block is also known as adaptive motor model in Figure 13 and it is used to calculate the motor torque, motor flux and position of stator flux space vector.

The Flux & Torque Hysteresis blocks contain a two-level hysteresis comparator for flux control and a three-level hysteresis comparator for the torque control. The Switching table block is the same as optimum pulse selector in Figure 4 and the input are signals from the output of the torque and flux hysteresis controllers.

A simulation is essential for studying advanced electric drive systems. After a careful review of the available software, many users consider MATLAB/Simulink to be ideal for this purpose [2]. The complex electrical drive control system is developed in SimPowerSystems. The dynamic simulation is one of the key steps in the validation of the system design phase of the electric motor drive systems. It also eliminates the drive control system design errors and the resulting errors before the real world implementation and testing [7].

SimPowerSystems contains libraries and analysis tools for modeling and simulating electrical power systems [8]. The libraries offer models of electrical power components, such as electrical machines, electric drives, electric machines, transformers, power converters and etc [8]. Application-specific libraries are also provided, it allows users to model specific types of electrical drives. Under Electric Drives/AC drives Library, a direct torque and flux control induction motor drive model is included. This significantly simplified the development time of the simulation model. After the model is developed, the dynamics system level performance can be simulated and tested in a single user friendly environment.

There are a lot of papers published that use SimPowerSystems for their simulation [22]-[25]. Therefore, the SimPowerSystems simulation software is selected to perform the analysis.



### 3.3.2 Induction Motor Dynamic Models used in Simulation

The induction motor is truly the workhorse of the industrial world and the traditional analysis of induction machines is presented in per phase equivalent circuits [5]. The operating principle of the induction motor, developed in terms of per phase equivalent circuit, is limited to the steady state analysis of the machine. It is very useful for studying the machine steady state performance. Steady state, in motor application, means that all electrical transients are ignored when frequency variations and sudden load changes occur [7]. However, such variations happen very often in variable frequency drives (VFD) application [7]. The induction motor dynamic model is usually required for electrical drive system analysis. During the design stage, simulation is one of the key steps in the validation of the design process of the motor drive system. It identifies design errors and the any errors in the prototype construction and testing. Hence he need for dynamic models of the induction machines [7]. The evaluation is needed so that the dynamics behaviour of VFD can be assessed. The instantaneous effects of varying voltages and currents, stator frequency, and torque disturbance are considered in the dynamic model.

The dynamic equations in arbitrary reference frame of induction machines in a matrix formed as in Eq. (3.15) [5].

$$\begin{bmatrix} v_{ds} \\ v_{qs} \\ v_{dr} \\ v_{qr} \end{bmatrix} = \begin{bmatrix} r_s + L_s p & -\omega L_s & L_m p & -\omega L_m \\ \omega L_s & r_s + L_s p & \omega L_m & L_m p \\ L_m & -(\omega - \omega_r) L_m & r_r + L_r p & -(\omega - \omega_r) L_r \\ (\omega - \omega_r) L_m & L_m p & -(\omega - \omega_r) L_r & r_r + L_r p \end{bmatrix} \begin{bmatrix} i_{ds} \\ i_{qs} \\ i_{dr} \\ i_{qr} \end{bmatrix} \quad (3.15)$$

Replacing  $p$  by  $\frac{d}{dt}$ , equation (3.15) can be written in scalar form:

$$v_{ds} = r_s i_{ds} + \frac{d\psi_{ds}}{dt} - \omega \psi_{qs} \quad (3.16)$$

$$v_{qs} = r_s i_{qs} + \frac{d\psi_{qs}}{dt} + \omega \psi_{ds} \quad (3.17)$$

$$v_{dr} = r_r i_{dr} + \frac{d\psi_{dr}}{dt} - (\omega - \omega_r) \psi_{qr} \quad (3.18)$$

$$v_{qr} = r_r i_{qr} + \frac{d\psi_{qr}}{dt} + (\omega - \omega_r) \psi_{dr}. \quad (3.19)$$

The flux linkages are shown in Eq. (3.20)-(3.23).

$$\psi_{ds} = L_s i_{ds} + L_m i_{dr} \quad (3.20)$$

$$\psi_{qs} = L_s i_{qs} + L_m i_{qr} \quad (3.21)$$

$$\psi_{dr} = L_r i_{dr} + L_m i_{ds} \quad (3.22)$$

$$\psi_{qr} = L_r i_{qr} + L_m i_{qs} \quad (3.23)$$

The equation of mechanical motion is

$$T_e - T_L = J \frac{d\omega_r}{dt}. \quad (3.24)$$

Electromagnetic torque can be expressed in terms of stator flux and stator current as:

$$T_e = \frac{3}{2} \frac{P}{2} (\psi_{ds} i_{qs} - \psi_{qs} i_{ds}). \quad (3.25)$$

DTC is expressed in a stationary reference frame applied to the squirrel cage induction motor and the equations become:

$$v_{ds}^s = r_s i_{ds}^s + \frac{d\psi_{ds}^s}{dt} \quad (3.26)$$

$$v_{qs}^s = r_s i_{qs}^s + \frac{d\psi_{qs}^s}{dt} \quad (3.27)$$

$$0 = r_r i_{dr}^s + \frac{d\psi_{dr}^s}{dt} + \omega_r \psi_{qr}^s \quad (3.28)$$

$$0 = r_r i_{qr}^s + \frac{d\psi_{qr}^s}{dt} - \omega_r \psi_{dr}^s \quad (3.29)$$

$$\psi_{ds}^s = L_s i_{ds}^s + L_m i_{dr}^s \quad (3.30)$$

$$\psi_{qs}^s = L_s i_{qs}^s + L_m i_{qr}^s \quad (3.31)$$

$$\psi_{dr}^s = L_r i_{dr}^s + L_m i_{ds}^s \quad (3.32)$$

$$\psi_{qr}^s = L_r i_{qr}^s + L_m i_{qs}^s \quad (3.33)$$

$$T_e = \frac{3}{2} \frac{P}{2} (\psi_{ds}^s i_{qs}^s - \psi_{qs}^s i_{ds}^s). \quad (3.34)$$

Combining Equations (3.26) and (3.30) becomes

$$v_{ds}^s = r_s i_{ds}^s + L_s \frac{di_{ds}^s}{dt} + L_m \frac{di_{dr}^s}{dt}. \quad (3.35)$$

Combining Equations (3.27) and (3.31) becomes

$$v_{qs}^s = r_s i_{qs}^s + L_s \frac{di_{qs}^s}{dt} + L_m \frac{di_{qr}^s}{dt}. \quad (3.36)$$

Combining Equations (3.28) and (3.32) becomes

$$0 = L_m \frac{di_{ds}^s}{dt} + \omega_r L_m i_{qs}^s + r_r i_{dr}^s + L_r \frac{di_{dr}^s}{dt} + \omega_r L_r i_{qr}^s. \quad (3.37)$$

Combining Equations (3.29) and (3.33) becomes

$$0 = -\omega_r L_m i_{ds}^s + L_m \frac{di_{qs}^s}{dt} - \omega_r L_r i_{qr}^s + r_r i_{qr}^s + L_r \frac{di_{qr}^s}{dt}. \quad (3.38)$$

Substitute Equations (3.30) and (3.31) into Equation (3.34) becomes

$$J \frac{d\omega_r}{dt} = \frac{3}{2} \frac{P}{2} [i_{qs}^s (L_s i_{ds}^s + L_m i_{dr}^s) - i_{ds}^s (L_s i_{qs}^s + L_m i_{qr}^s)] - T_L. \quad (3.39)$$

Equations (3.35) to (3.39) are a set of differential equations are used to build the induction machines model for further analysis.

## Chapter 4: Problem Definition, Solution and Simulations

### 4.1 Problem Definition

In case of a cobble occurring, the shears starts and runs continuously to cut the material into small pieces. If the bar is very long; the requirement of shear cobble cutting time will be long also.

By conducting field measurements it was identified that, during cobble cutting mode, the speed reference ramped up in a similar profile to the normal cutting mode (Figure 14). When the speed reference ramps up in a short time, a speed error signal and a high torque reference is created in order to minimize the speed error. This causes current spikes during the acceleration and deceleration in a short period of time.

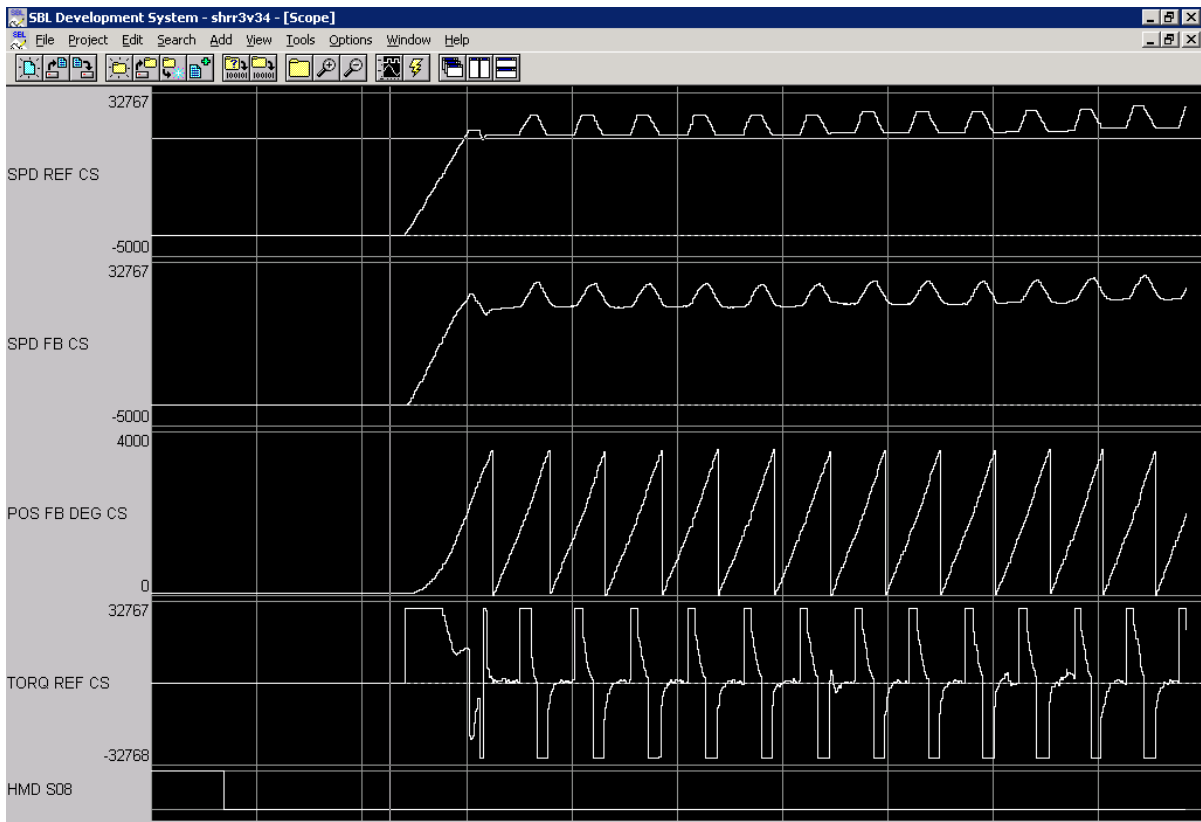


Figure 14: Real World System Result (Pre-Modification)

It was realized that position control is not necessary during cobble cutting because the accuracy of bar length and the quality of the bar is not as important as with normal cutting. The chopped bar is discarded after cobble cutting. By controlling the drive with a constant speed reference, in cobble cutting mode, the torque reference is not as high because the speed error is much less. The current level is lower, according to equation (3.2), and less heat is generated.

The induction motor DTC model has been developed in Matlab/SimPowerSystems for simulation and it is shown in Figure 15.

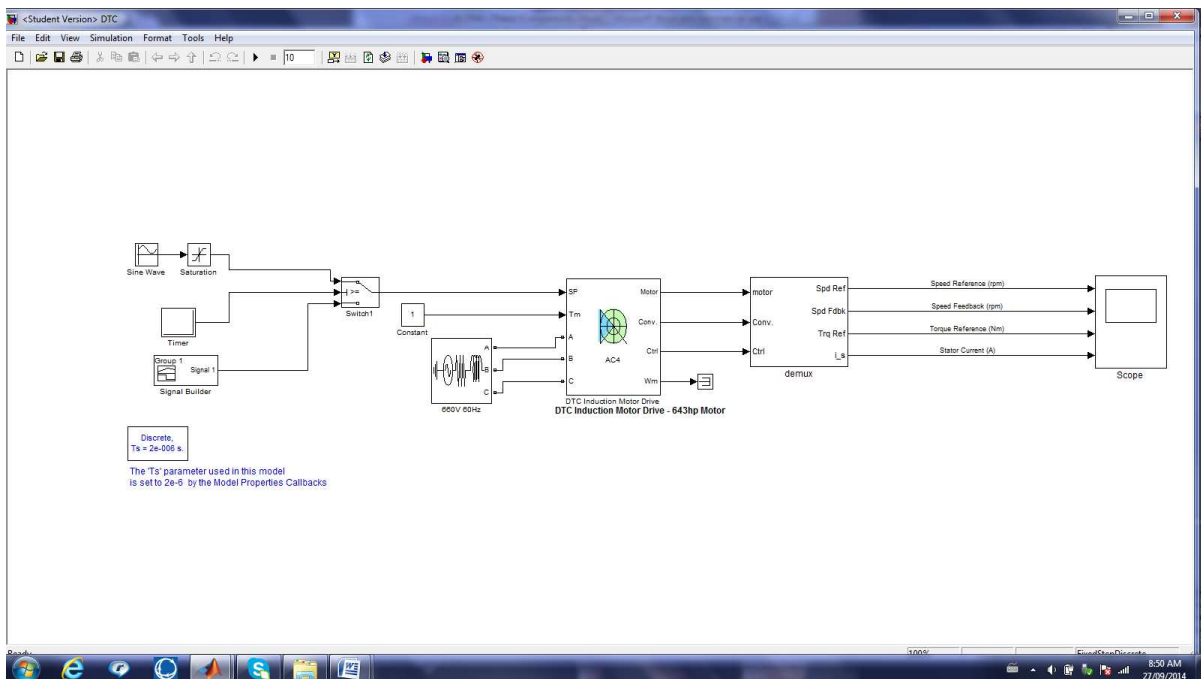


Figure 15: Simulation Model

The simplified DTC drive and motor block diagram has been used in Matlab/SimPowerSystems software. The power input to the DTC block is a three phase 660V power supply. The speed reference is programmed such that it will produce the initial speed ramp up and then automatically switch to speed up/down motion in order to simulate the speed profile of the CCS. The Demux block is SimPowerSystems prebuilt machine

measurement demultiplexer that is used to split measurement signal of machine models into separate signals. In this case, it extracts speed reference, speed feedback, torque reference and stator current from the DTC induction motor Drive block. These separated signals are then fed into the Scope (Figure 15).

Motor Nameplate Data and Parameters are input into the model as follow (Figure 16):

- $Power = 643hp$
- $Voltage = 660V$
- $I_n = 549A$
- $\omega_n = 1200rpm$
- $p.f. = 0.80$
- $\eta = 95.3\%$
- $\tau = 3817N \cdot m$
- $r_s = 0.0233\Omega$
- $L_{ls} = 0.239mH$
- $r_r = 0.0087\Omega$
- $L_{lr} = 0.249mH$
- $L_m = 3.99mH$

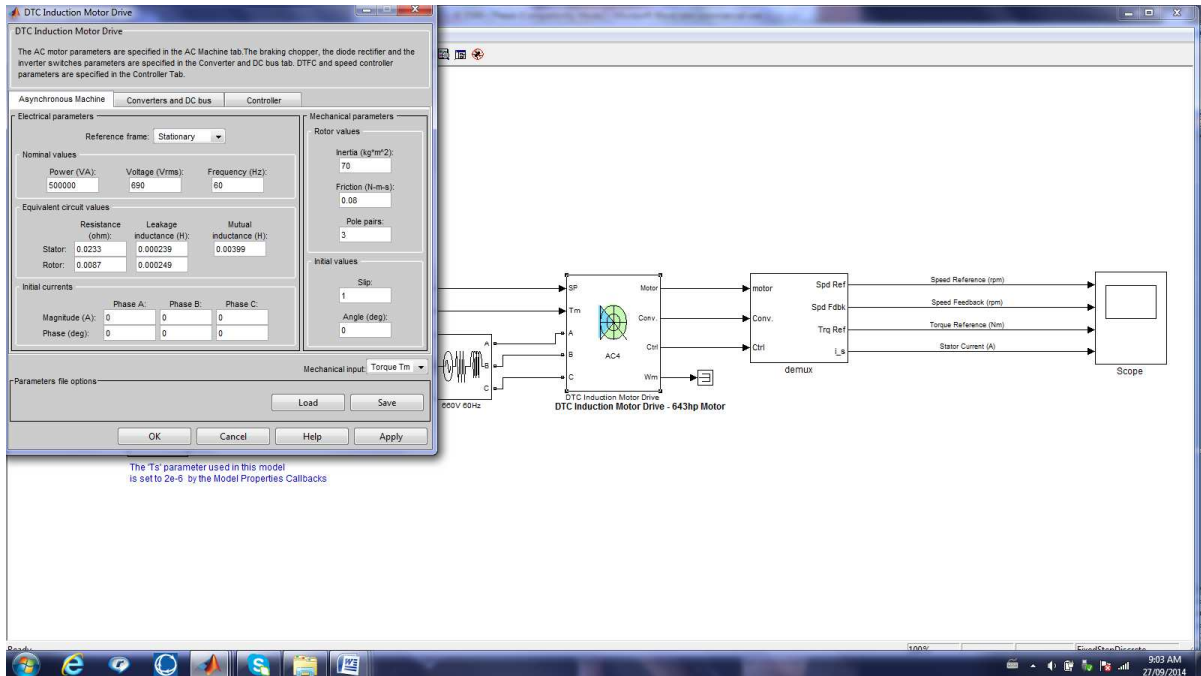


Figure 16: Induction Motor Information Parameters

After all the information is input into the system, the scope is set up such that it will run for 10 seconds with all y-axis data correctly scaled. Referring to Figure 17, the results of the simulation are shown for the pre-modification case. The speed feedback follows the speed reference very closely. Since the speed reference changing up/down frequently, the speed regulator tries to keep the speed error to minimum, therefore, it results in a 300% (maximum) torque. This graph agrees with the actual system behavior shown in Figure 14. When the stator current trend is added (the Figure 17 – Trend #4) it clearly shows that during the speed ramp up/down, there are some current pulses generated. It is these current pulses that creating the excessive heat and exceed the drive thermal limit, causing the fault condition in the DTC.

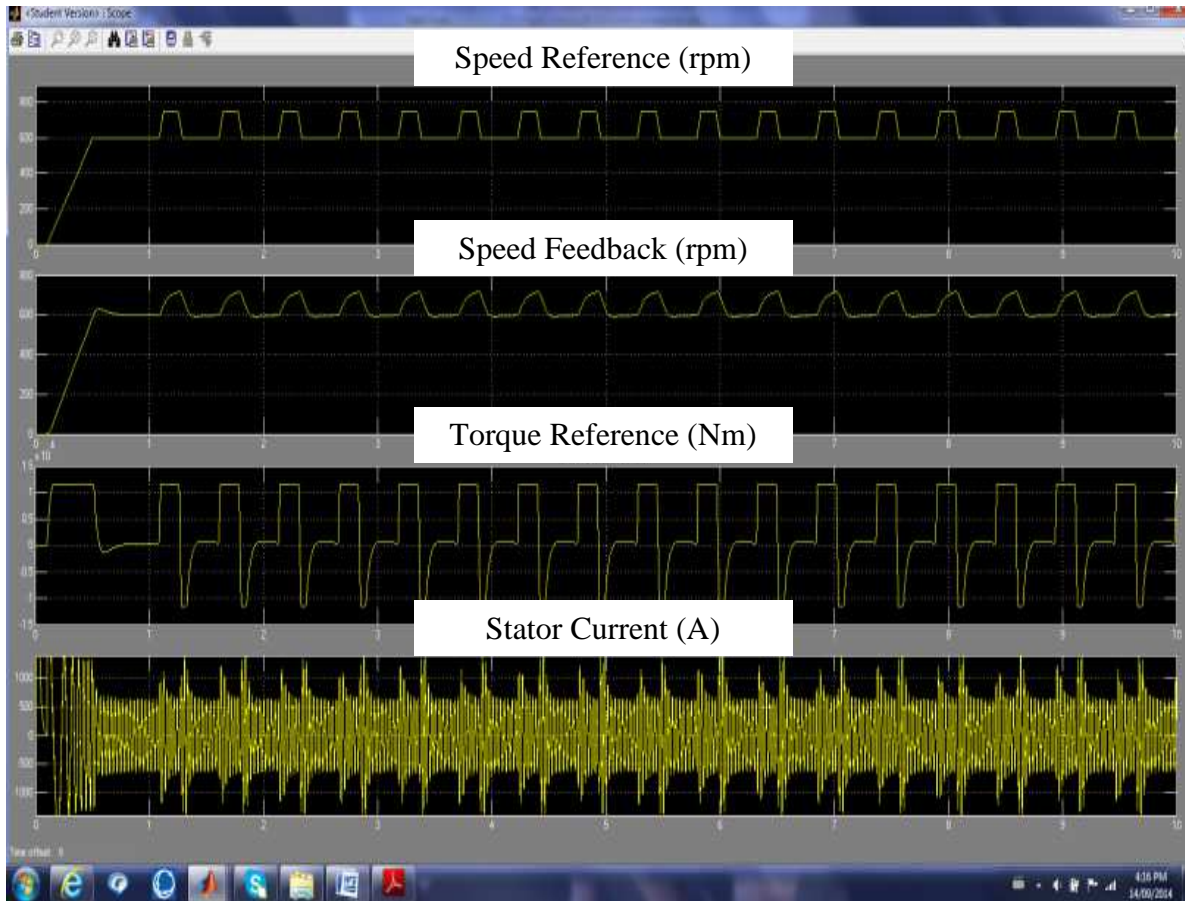


Figure 17: Simulation Result (Pre-Modification)

The DTC drive provides an  $I^2t$  overload protection and is based on a thermal model [26]. Figure 18 shows how the system provides overload protection [28]–[31]. In this case, the CCS motor has a full load current of 549A and the drive allows for an overload conditions for a short time defined as follow:

- 150% Overload – allow 1 min every 5 mins
- 200% Overload – allow 10 sec every 60 sec



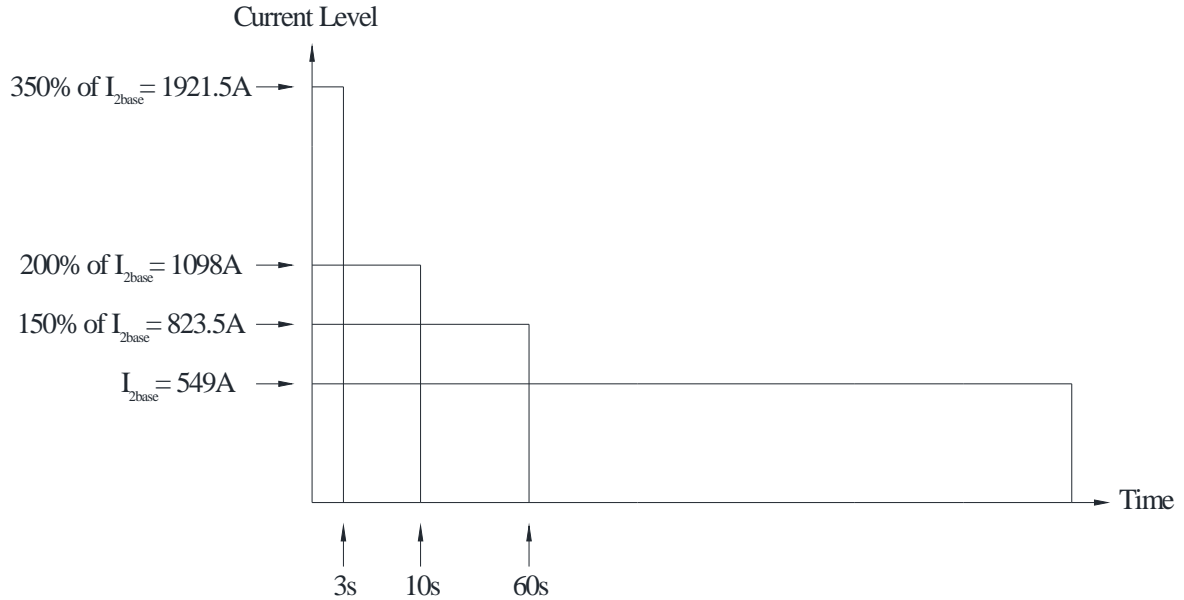


Figure 18: Output Current Overload Characteristic Graph

The CCS DTC system is considered to be a heavy duty application and during the acceleration period since the torque will increase by 300% of rated torque and current will increase by almost 200% of rated current (Figure 17 – Trend #4). Therefore, in this case a 200% overload will be considered.

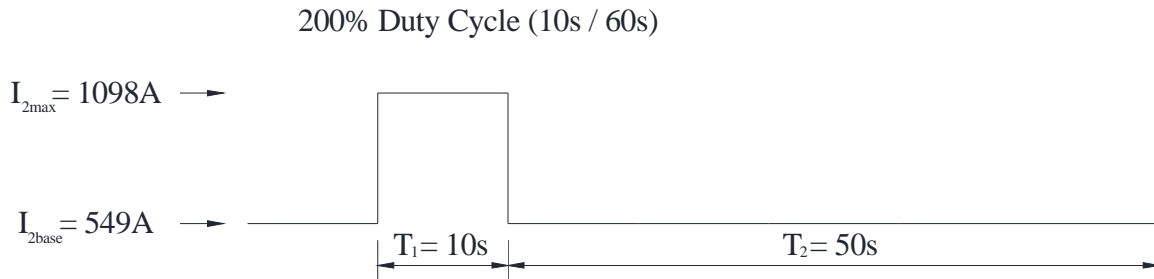


Figure 19: DTC Drive 200% Duty Cycle

As shown in Figure 19,  $I_{2base} = 549A$  and  $I_{2max} = 1098A$  for a duty cycle of 10s/60s. The approximate average thermal limit of the DTC Inverter Section with 60 seconds interval is calculated as follow:

$$\begin{aligned}
&= I_{2_{\max}}^2 (T_1) + I_{2_{\text{base}}}^2 (T_2) \\
&= (1098 A)^2 (10 s) + (549 A)^2 (50 s) = 27.13 \times 10^6 A^2 \cdot \text{sec}
\end{aligned}$$

Approximations for the average thermal dissipation of the DTC drive during cobble cutting is

$$\begin{aligned}
&= I_{\text{ramp}}^2 (T_1) + I_{\text{const}}^2 (T_2) \\
&= (920 A)^2 (24 s) + (450 A)^2 (36 s) = 27.60 \times 10^6 A^2 \cdot \text{sec}
\end{aligned}$$

The above calculations show that, during cobble cutting, the thermal dissipation exceeds the thermal limit of the DTC drive and causes the drive faults due to an overcurrent.

## 4.2 Solution and Simulations

The proposed solution is to reduce the width of the torque pulses or even eliminated these pulses completely. This will result in the current drawn being lower and the current spikes will be eliminated. It follows that the thermal dissipation will be lower and should be below the thermal limit of the DTC drive.

The simulation shows that after the speed reference is changed to a constant (Figure 20), the torque pulses are almost completely eliminated, except for the initial acceleration and the minimum torque that is required to maintain the CCS rotation. Note that the current spikes are also eliminated (Figure 20 – Trend #4)

After these modifications, the estimated average thermal dissipation of the drive during cobble cutting becomes:

$$\begin{aligned}
&= I_{\text{acc\_dec}}^2 (T_1) + I_{\text{const}}^2 (T_2) \\
&= (0 A)^2 (0 s) + (450 A)^2 (60 s) = 12.15 \times 10^6 A^2 \cdot \text{sec}
\end{aligned}$$

The calculation shows that the heat dissipation is significantly reduced from  $27.60 \times 10^6 A^2 \cdot \text{sec}$  to  $12.15 \times 10^6 A^2 \cdot \text{sec}$  after the changes are implemented. The new calculated value is well below the thermal limit  $27.13 \times 10^6 A^2 \cdot \text{sec}$  of the DTC drive.

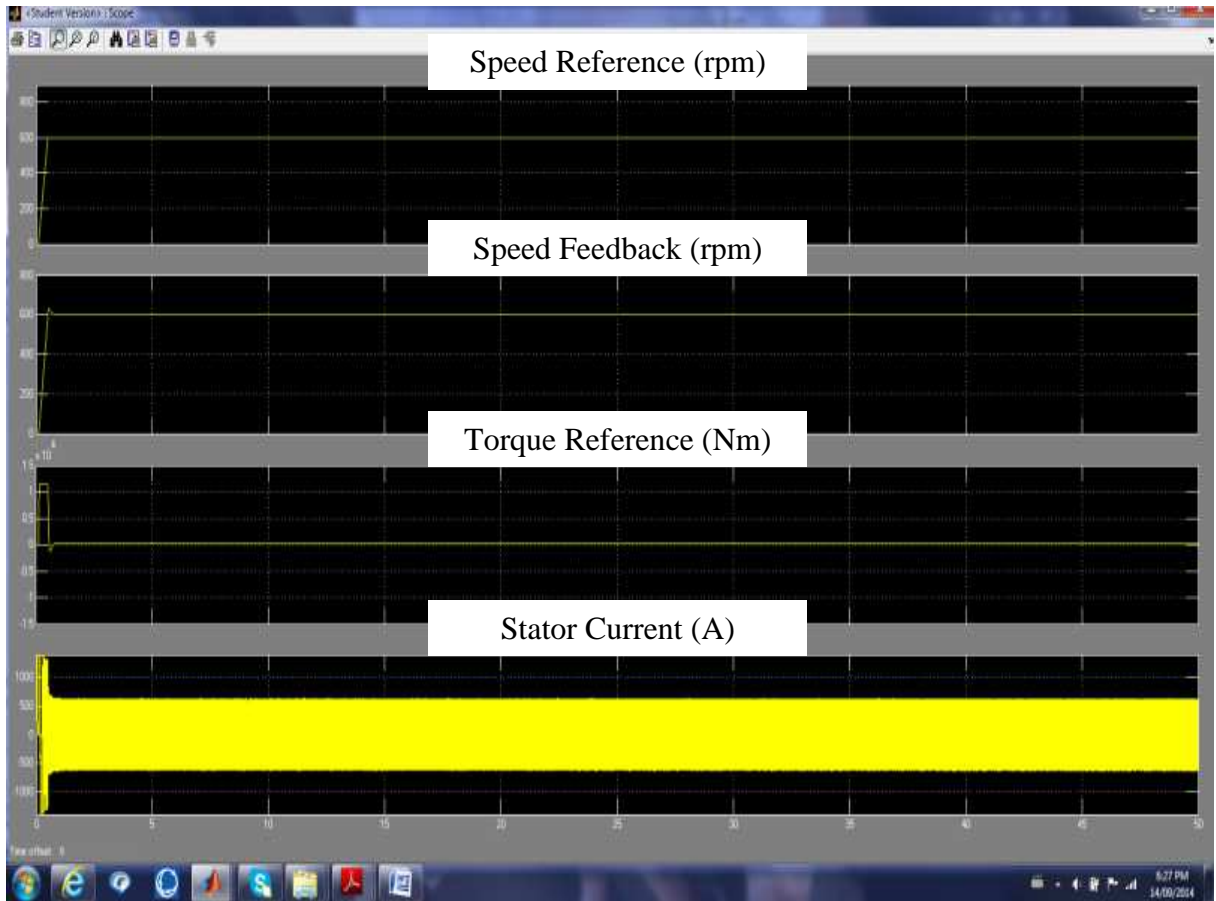


Figure 20: Simulation Result (Post-Modification)

## Chapter 5 – System Design

### 5.1 CCS System Overview

Following the successful simulation results from previous chapter that predicted the proposed solution would correct the over-current fault condition in the concept, the actual design and modification of the existing system is required. In Figure 21, it shows the existing CCS DTC motor drive control system block diagram.

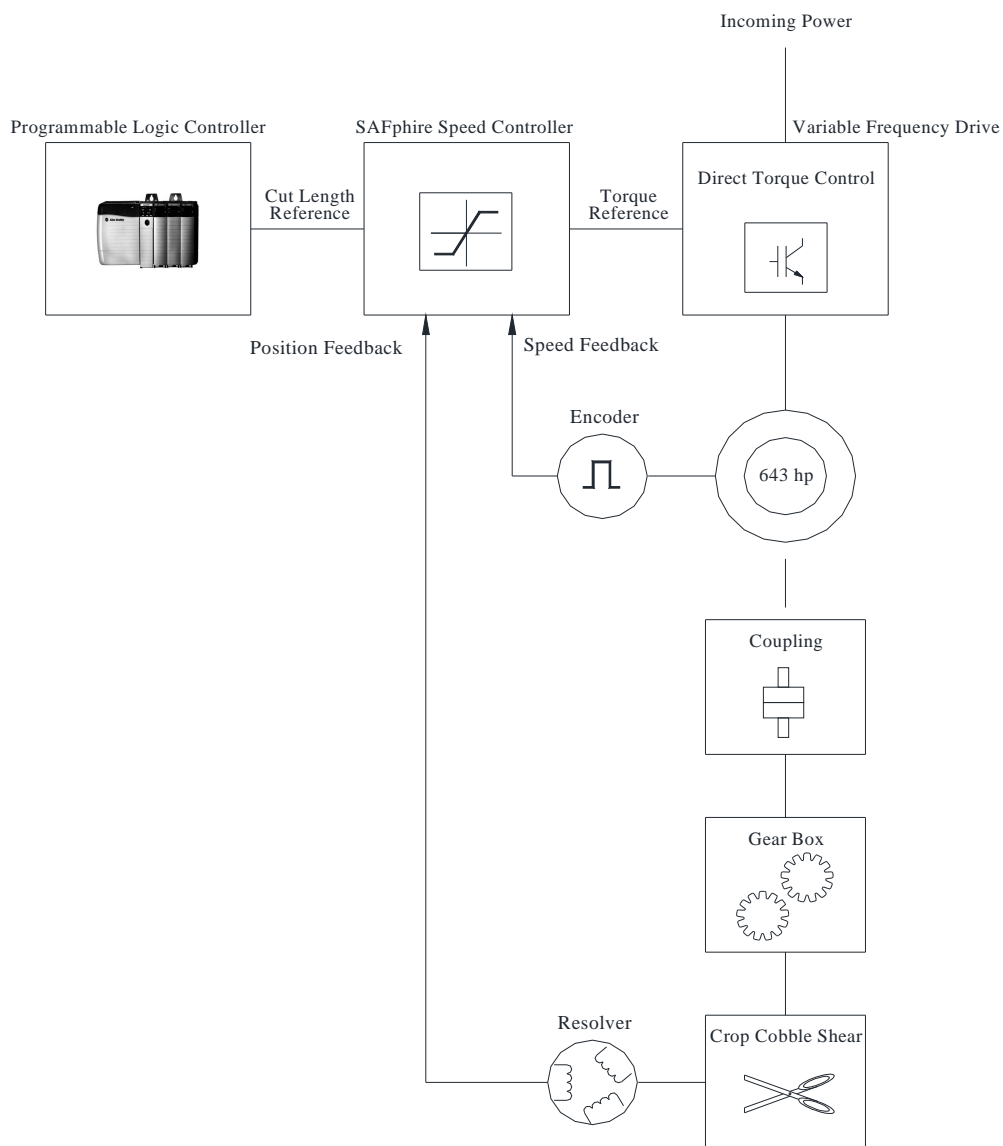


Figure 21: CCS DTC Control Block Diagram

Refer to Figure 21, the DTC acts as a torque amplifier as it is programmed in a torque regulation or control mode. The input is the torque reference and this comes from the high level speed controller. This speed controller named SAFphire is where the PI type speed control loop is housed [32]-[34]. Therefore, there are no changes required in the DTC drive. The only modification required is to the speed reference generator within the SAFphire speed controller.

## 5.2 SBL Programming

### 5.2.1 Introduction to SBL

SAFphire Programmable Linear Controller (Figure 22) is a DSP based controller designed for closed-loop drive control applications. It can perform high-performance servo-like tension and position control [32]. The Real-time graphical "Control Block Concept" Windows-based programming language called SAF Block Language (SBL) is used to make the modification to the speed reference.



Figure 22: CCS SAFphire System

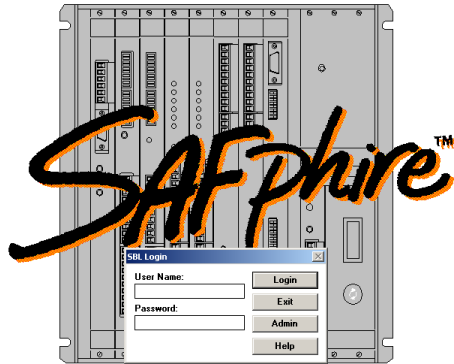


Figure 23: SAFphire SBL Software [32]

### 5.2.2 CCS SAFphire Modeling

One of the main responsibilities of SAFphire is controlling the position of the shear blade. SAFphire models the CCS in terms of the blade position and the actual blade position is constantly fed back to the SAFphire controller by resolver (Figure 21). Viewed from directly in front of the shear (Figure 24), the CCS blade position can be viewed as Figure 25.



Figure 24: Crop Cobble Shear Front View

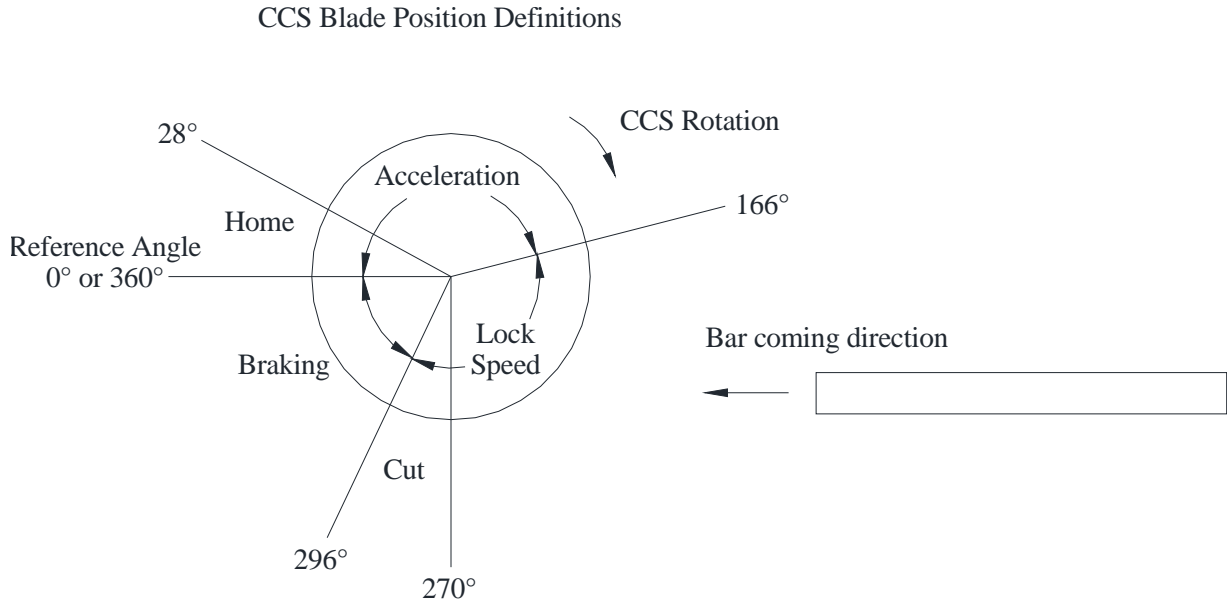


Figure 25: CCS Blade Position

The blade position angles are defined as follow:

- $0^\circ$  or  $360^\circ$  - Reference Angle
- $0^\circ$  to  $28^\circ$  - Home Range
- $0^\circ$  to  $166^\circ$  - Acceleration Region
- $166^\circ$  to  $296^\circ$  - Lock Speed Region (Constant High Speed Region)
- $270^\circ$  to  $296^\circ$  - Cut Range
- $296^\circ$  to  $360^\circ$  - Braking Region

Normally, the shear is rested at home range  $0^\circ$  to  $28^\circ$  and waiting for the bar to arrive. When the shear receives the start signal from Hot metal detector (HMD); the shear accelerates to a high speed before the angle of  $166^\circ$  is reached (acceleration region  $0^\circ$  to  $166^\circ$ ). After  $166^\circ$ , the shear enters into lock speed region, which is essentially an overspeed region. The lock speed signal is triggered and the shear accelerates to a preset higher speed. This higher speed is required at the moment of cutting the bar since, when the blade first hits the bar, the CCS

blade will slow down due to the impact force. The overspeed acts as speed drop compensation to ensure the CCS has enough speed to cut through the bar without slowing down significantly. If the shear blade slows down too much during cutting, it may cause an inaccuracy of the cut length or in the extreme, the blade may be stalled in the middle of the cutting process which will create a cobble. In practice, the shear blade will strike the bar between  $270^{\circ}$  to  $296^{\circ}$ , therefore, in the SAFphire program, it is defined as the cut range. After the shear finishes the cut, the lock speed signal will release and the shear enters into the braking (deceleration) region and stops at the home position.

During the cobble cut (continuous cutting), when the shear receives the cobble signal, the shear accelerates to the reference speed within the acceleration region ( $0^{\circ}$  to  $166^{\circ}$ ). The operation is similar to the normal single cut described above and the difference is after the cut, the shear will not enter the braking region. Instead, it will decelerate to the reference speed until the angle reaches  $166^{\circ}$  again. Then the lock speed signal is triggered and the shear accelerates again. The cycle continues until the cobble signal is no longer active.

### **5.2.3 SBL Program Modification**

The objective of the modification is to focus on the lock speed signal. If the lock speed signal is bypassed during the cobble cut mode, then the speed reference becomes constant. The modification will be accomplished in two steps:

1. The signal is traced back from the ABB DTC Drive to Lock Speed Signal (Figure 26 to Figure 29).
2. The modification on the Lock Speed Signal (Figure 30).



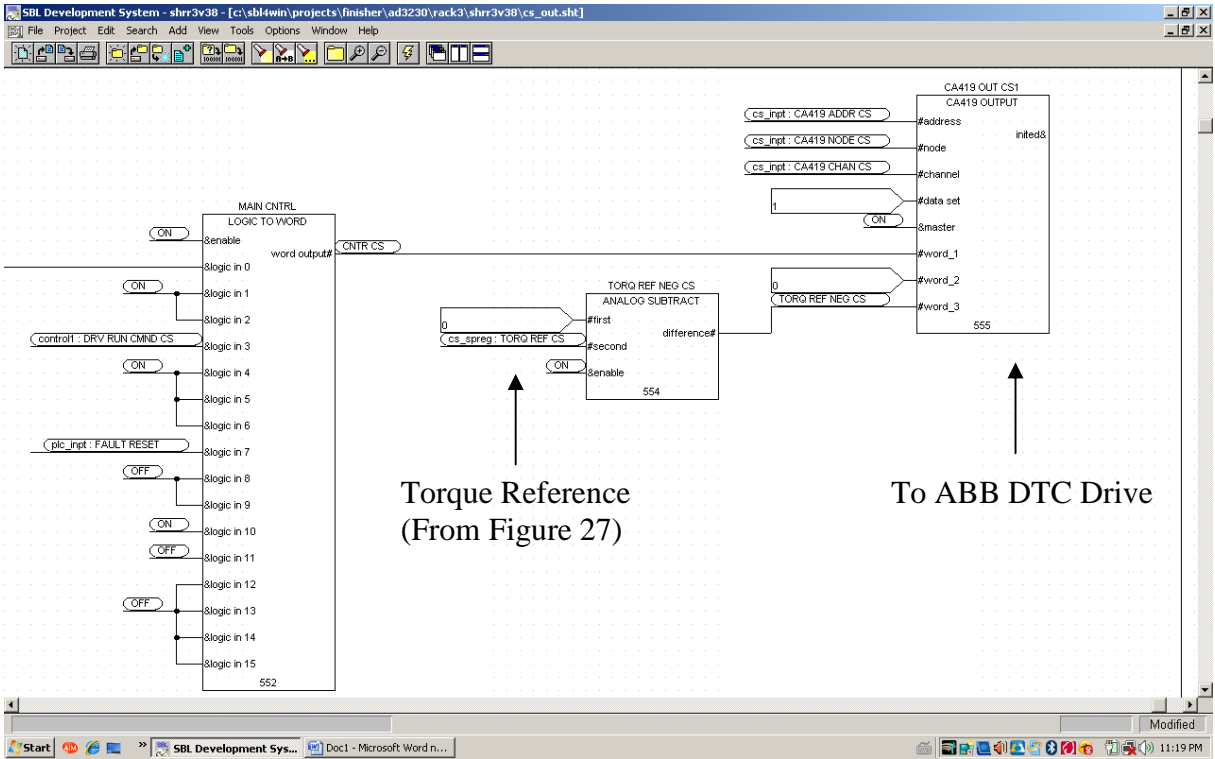


Figure 26: CCS Speed Controller Output

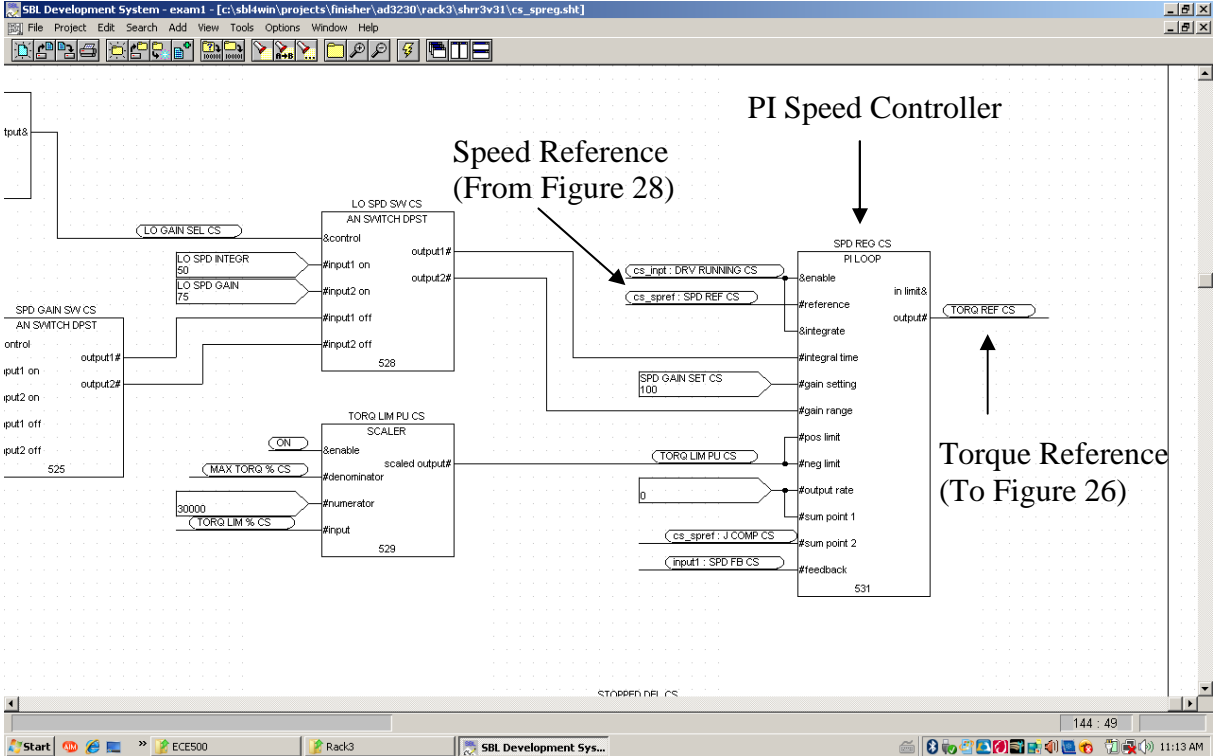


Figure 27: CCS Speed Controller

SAFphire's PI speed control loop for CCS is shown in Figure 27. The input to the speed regulator is the speed reference and the output is the torque reference which sends a signal to the ABB DTC drive (Figure 26). In Figure 28, the speed reference can be traced back to the signal CLMP SPD REF CS. Then the signal CLMP SPD REF CS can be further traced back to the speed reference signal SPD FB S7/8 (Figure 29). In Figure 29, it shows that the speed reference is SPD FB S7/8 and it is controlled by both cobble signal COBBLE HEAD and the lock speed signal LOCK SPD CS. Therefore, the modification is performed such that during the cobble condition (COBBLE HEAD), the lock speed signal (LOCK SPD CS) is bypassed (See Figure 30).

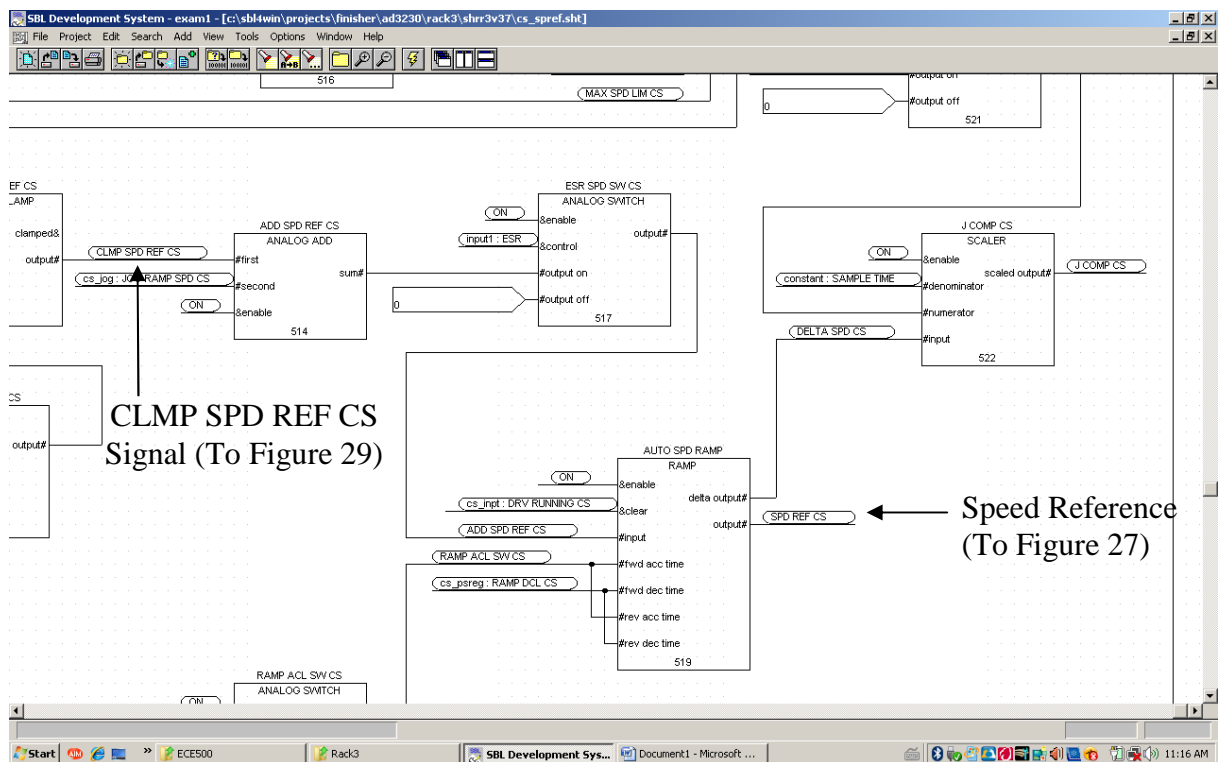


Figure 28: CCS Speed Reference

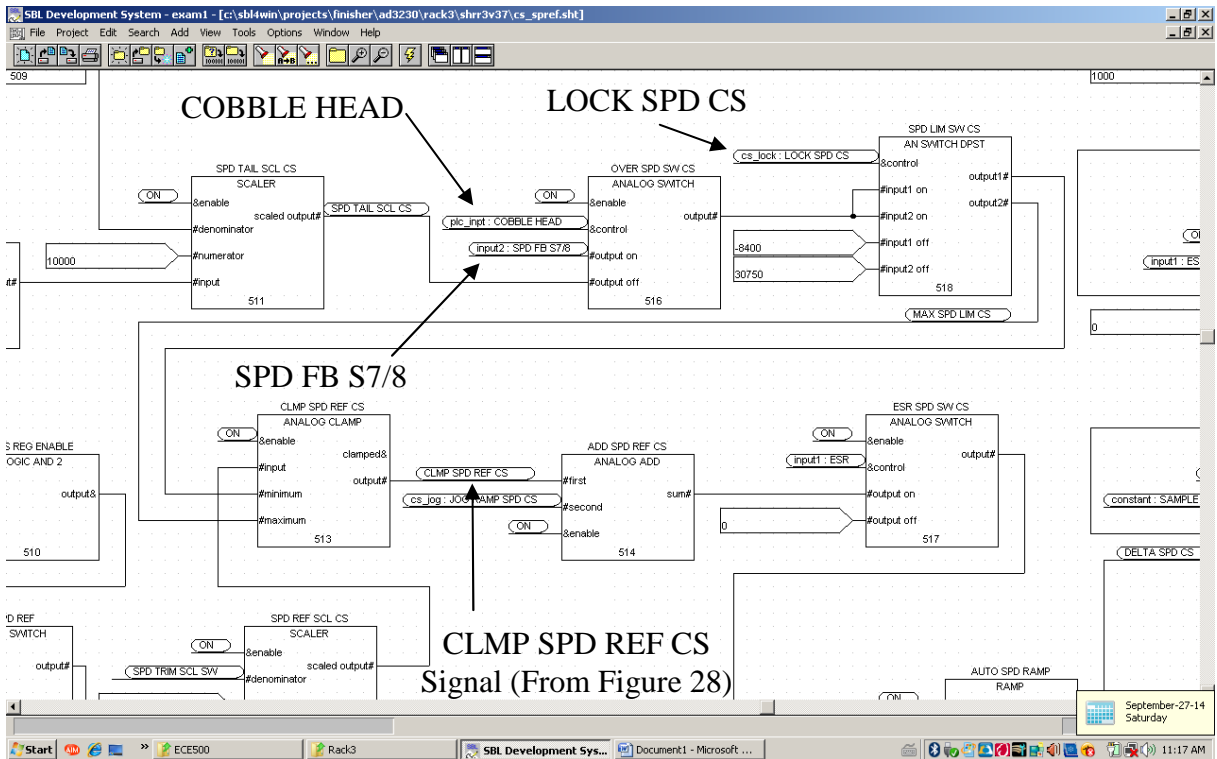


Figure 29: CCS Lock Speed (Pre-Modification)

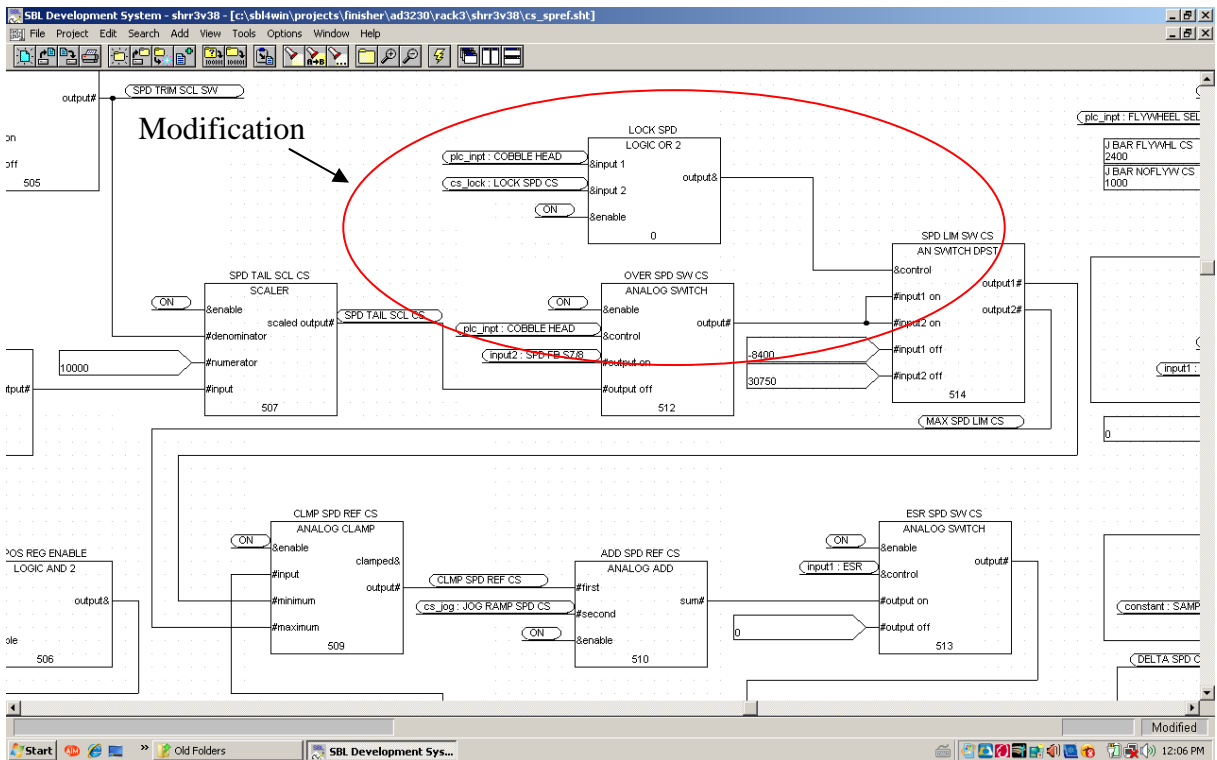


Figure 30: CCS Lock Speed (Post-Modification)

## Chapter 6 – Results from the Physical System

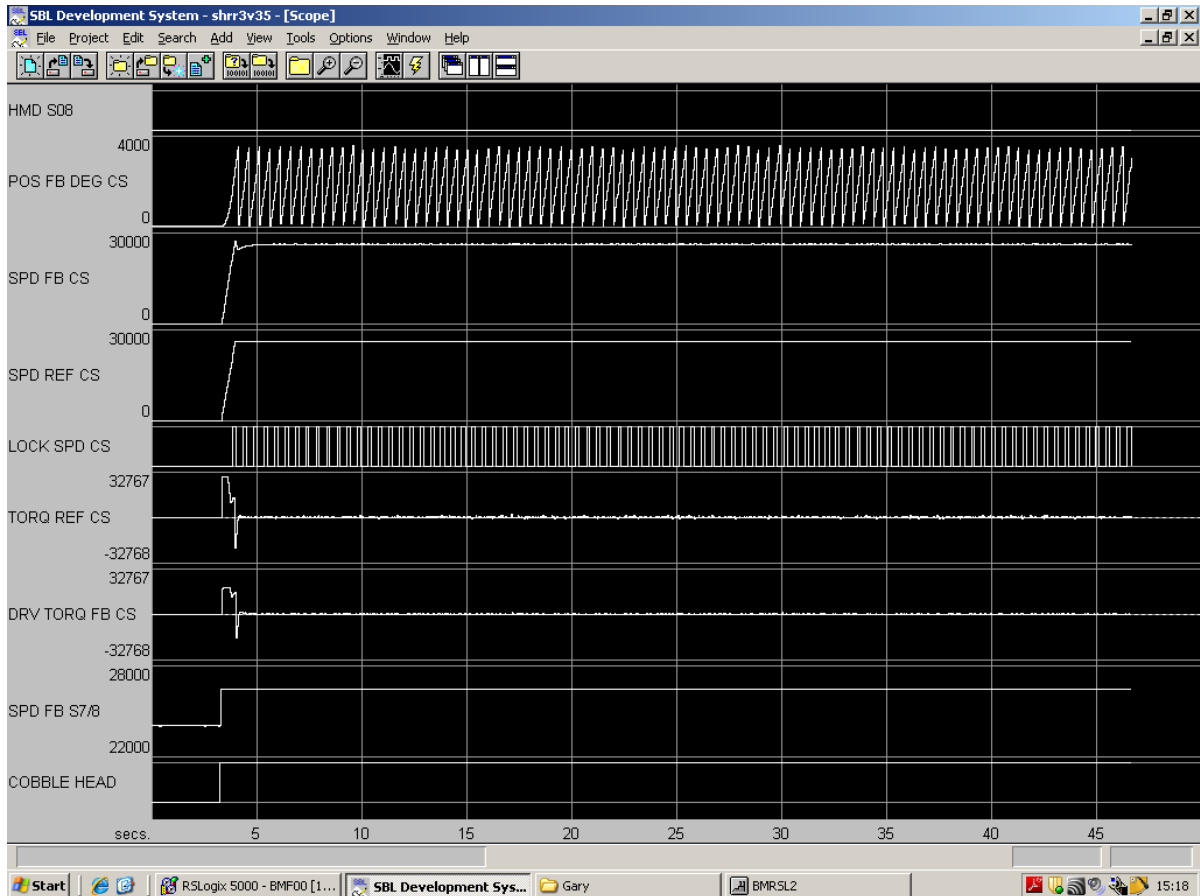


Figure 31: Real System Result (Post-Modification)

After the modification is completed from previous chapter, the testing is performed and the recorded result is shown in Figure 31. The figure shows that the speed reference is constant even when the lock speed signal is still active. The results from the operational system show all torque pulses are eliminated, which implies that the current pulses are also eliminated during cobble cutting. This compares well with the simulation result (Figure 19). Following the testing of the modified system, the changes were permanently implemented into the system and the DTC drive overcurrent fault issue, during cobble cutting, was resolved.

## Chapter 7 – Conclusion and Future Recommendation

### 7.1 Conclusion

The speed ramping up/down during CCS cobble cutting caused the overcurrent faults in the DTC drive. This speed ramp is not required since the length of the bar and the bar head quality is not important. The improvement to the cobble cutting control is to make the speed reference constant. After gathering the practical data (Figure 13), a simulation was performed to better understand why the fault current occurs (Figure 16). In general, experimental data from measurements on the system in the steel mill are compared favorably with simulation results. The comparison between simulated and measured results shows that the simulation closely models the physical system. So the system has been accurately simulated and this provides a model that allows for the determination of a suitable approach for improving CCS DTC drive operation.

The constant speed reference simulation is also performed (Figure 19). The result shows that current spikes are eliminated. The modifications were made to the system and measurements are carried out to verify the improvement. The final implementation regarding the reference torque profile shows that the torque pulses are also eliminated (Figure 31). This significantly reduces the thermal dissipation within the DTC drive. The calculation shows that the thermal dissipation of the modified system is below the thermal limit of the DTC drive. Therefore, the modification of the CCS operation successfully eliminated the frequent faults previously encountered. The elimination of this fault is understood to have saved AltaSteel approximate \$1,000,000 in capital expenditure that would have been incurred if they had upgraded to a larger motor drive system. This estimate does not include lost production time as well as maintenance and repair time.

## **7.2 Future Recommendation**

In the existing CCS motor drive control system, the speed regulator is housed inside the SAFphire high speed controller (Figure 21). However, this specific configuration is not fully utilizing the capability of the DTC drive. Research should be conducted in this area to investigate if the system can be configured to use the speed controller inside the DTC drive. Therefore, the SAFphire controller may not be required. The system would be less complex, would potentially offer better performance and provide better reliability.

## References

- [1] Abu-Rub, H., Iqbal, A., Guzinski, J. (2012). High Performance Control of AC Drives (1<sup>st</sup> ed). West Sussex: John Wiley & Sons Ltd.
- [2] Mohan, N., (2014). Advanced Electric Drives: Analysis, Control, and Modeling Using MATLAB/Simulink Simulations. Hoboken: John Wiley & Sons Ltd.
- [3] Bose, B., (2002). Modern Power Electronics and AC Drives (1<sup>st</sup> ed). Upper Saddle River: Prentice Hall.
- [4] Vas, P., (1998). Sensorless Vector and Direct Torque Control (1<sup>st</sup> ed). New York: Oxford University Press.
- [5] Lipo, T., Novotny, D., (1996). Vector Control and Dynamics of AC Drives (1<sup>st</sup> ed). New York: Oxford University Press.
- [6] Jahns, T., Lipo, T., Novotny, D., (2009). Introduction to Electric Machines and Drives (1<sup>st</sup> ed). Madison: University of Wisconsin – Madison.
- [7] Krishnan, R., (2001). Electric Motor Drives Modeling, Analysis and Control (1<sup>st</sup> ed). Upper Saddle River: Prentice Hall.
- [8] Tyagi, A., (2012). MATLAB and Simulink for Engineers (1<sup>st</sup> ed). New York: Oxford University Press.
- [9] MathWorks (2014). DTC Induction Motor Drive. Retrieved from <http://www.mathworks.com/help/physmod/sps/powersys/ref/dtcinductionmotordrive.html>.
- [10] Patra, N., (2013). Study of Induction Motor Drive with Direct Torque Control Scheme and Indirect Field Oriented Control Scheme using Space Vector Modulation. Retrieved from <http://ethesis.nitrkl.ac.in/5162/1/211EE2136.pdf>.
- [11] Manuel, A., Francis, J., (2013). Simulation of Direct Torque Control Induction Motor Drive by using Space Vector Modulation for Torque Ripple Reduction. Journal of International Journal of Advanced Research in Electrical, Electronics and Instrumentation Engineering, 2(9), 4471-4478.
- [12] Lazarini, M., Filho, E., (2007). Sensorless three-phase induction motor direct torque control using sliding mode control strategy laboratory set-up for motor speed control teaching. Journal of International Conference on Engineering Education.

- [13] Allirani, S., Jagannathan, V., (2010). High Performance Direct Torque Control of Induction Motor Drives Using Space Vector Modulation. *Journal of International Journal of Computer Science*, 7(6), 178-186.
- [14] Kumar, N., Singh, J., (2013). Direct Torque Control of Three Phase Induction Motor Using Matlab. *International Journal for Research in Applied Science and Engineering Technology*, 1(2), 16-186.
- [15] Hanfeng, S., Automation and control of wire rod finishing mill line. Zurich: ABB Ltd. Retrieved from [http://www05.abb.com/scot/scot267.nsf/veritydisplay/13db3dee24c79231852577c1000314c6/\\$file/abb\\_wirerod\\_13\\_lt-1.pdf](http://www05.abb.com/scot/scot267.nsf/veritydisplay/13db3dee24c79231852577c1000314c6/$file/abb_wirerod_13_lt-1.pdf).
- [16] Sainz, B., Swan, S. (2004), Cross Country Bar Mill Control Modernization at Nucor Marion. Retrieved from <http://prug.espacios.net.mx/amige/sitio/pdf/Microsoft%20Word%20-%20Cross%20Country%20Bar%20Mill%20Control1.pdf>.
- [17] Danieli Automation, Large drives system solutions for challenging metals plants applications. Retrieved from [http://www.dca.it/Libraries/Papers/Large\\_drives\\_system\\_solutions.sflb.ashx](http://www.dca.it/Libraries/Papers/Large_drives_system_solutions.sflb.ashx).
- [18] Danieli Automation, QDrives Medium Voltage Drives. Retrieved from [http://www.dca.it/Libraries/QDrive\\_MV/QDRIVE\\_MV.sflb.ashx](http://www.dca.it/Libraries/QDrive_MV/QDRIVE_MV.sflb.ashx).
- [19] ABB Inc., ABB Drives and Control System for Hot Flat Rolling Mills Improves Yield and Quality. Retrieved from [http://www05.abb.com/global/scot/scot227.nsf/veritydisplay/38095ded87b035cac12570af00/3b8ab1/\\$file/seaisi2005\\_control%20and%20drive%20systems%20for%20hot%20flat%20rolling%20mills.pdf](http://www05.abb.com/global/scot/scot227.nsf/veritydisplay/38095ded87b035cac12570af00/3b8ab1/$file/seaisi2005_control%20and%20drive%20systems%20for%20hot%20flat%20rolling%20mills.pdf).
- [20] ABB Drives in Metals – Medium voltage drives for improved product quality and process control. Retrieved from [http://www05.abb.com/global/scot/scot227.nsf/veritydisplay/ae7e1f4046cbcf17482573950004815c/\\$file/abb\\_drives\\_in\\_metals\\_reva.pdf](http://www05.abb.com/global/scot/scot227.nsf/veritydisplay/ae7e1f4046cbcf17482573950004815c/$file/abb_drives_in_metals_reva.pdf).
- [21] Thorstenson, E., Drive Selection for Rolling Mills  
Retrieved from <http://www.russula.com/articles/article-04.php>.
- [22] Pimkumwong, N., Onkrong, A., Sapaklom, T. (2011), Modeling and Simulation of Direct Torque Control Induction Motor Drives via Constant Volt/Hertz Technique  
Retrieved from <http://www.sciencedirect.com/science/article/pii/S1877705812011903>



- [23] Craciunescu, A., Youb, L. (2011), Comparison by Simulation of Various Strategies of Three Level Induction Motor Torque Control Schemes for Electrical Vehicle Application. Retrieved from [http://www.iaeng.org/publication/WCE2011/WCE2011\\_pp1444-1449.pdf](http://www.iaeng.org/publication/WCE2011/WCE2011_pp1444-1449.pdf).
- [24] Koshy, M., Simulation of Direct Torque Control of Induction Motor Retrieved from [www.researchgate.net/dtc.pdf](http://www.researchgate.net/dtc.pdf).
- [25] Allirani, S., Jagannathan, V., Direct Torque Control Technique in Induction Motor Drives – A Review. Retrieved from <http://www.jatit.org/volumes/Vol60No3/2Vol60No3.pdf>.
- [26] ABB. (2011). Technical guide No. 1 Direct torque control – the world’s most advanced AC drive technology. Retrieved from [http://www05.abb.com/global/scot/scot201.nsf/veritydisplay/14f3a3ad8f3362bac12578a7004/1e728/\\$file/ABB\\_Technical\\_guide\\_No\\_1\\_REVC.pdf](http://www05.abb.com/global/scot/scot201.nsf/veritydisplay/14f3a3ad8f3362bac12578a7004/1e728/$file/ABB_Technical_guide_No_1_REVC.pdf).
- [27] ABB. (1996). Technical guide No. 100 High Performance Drives Speed and Torque Regulation. Retrieved from [http://www05.abb.com/global/scot/scot239.nsf/veritydisplay/8492cb383e941d57852571c3006b0194/\\$file/speedtorq.pdf](http://www05.abb.com/global/scot/scot239.nsf/veritydisplay/8492cb383e941d57852571c3006b0194/$file/speedtorq.pdf).
- [28] ABB. (2000). ACS 600 MultiDrive Safety and Product Information. Helsinki: ABB Industry Oy.
- [29] ABB. (1999). ACS 600 Firmware Manual. Helsinki: ABB Industry Oy.
- [30] Brown, M. (1997). Siemens Standard Drives Application Handbook
- [31] Rockwell Automation Inc. (2013). PowerFlex 70/700 Adjustable Frequency AC Drives Reference Manual. Milwaukee: Rockwell Automation
- [32] SAFphire. Retrieved from <http://www.safphire>.
- [33] SAF Drive Inc. SBL Programming Software – Software User Guide Retrieved from <http://www.safphire.com>.
- [34] SAF Drive Inc. SBL Programming Software – Block Descriptions (CA451) Retrieved from <http://www.safphire.com>.
- [35] Lannon, J., Klepp, D., (2006). Technical Communication (3<sup>rd</sup> ed). Toronto: Pearson.
- [36] Depenbrock, M., (1988). Direct Self Control (DSC) of Inverter fed Induction Machine. IEEE Transactions on Power Electronics, 3(4), 420-429.

## Appendices

### A. Project Pictures



Figure 32: Rolling Mill Electrician during Commissioning



Figure 33: Rolling Mill Operator during Commissioning



Figure 34: ABB CCS DTC Drive

## B. ABB ACS600 Drives Model, Parameters and Ratings

Model: ACA 610-1385-6

Parameters Number	Parameter Name	Settings
99.01	Language	ENG AM
99.02	Application Marcos	Torque Control
99.04	Motor Control Mode	DTC
99.05	Motor Nominal Voltage	660Vac
99.06	Motor Nominal Current	549A
99.07	Motor Nominal Frequency	60Hz
99.08	Motor Nominal Speed	1200rpm
99.09	Motor Nominal Power	643hp
10.01	EXT1 Start/Stop/Direction	Not Sel
10.02	EXT2 Start/Stop/Direction	Comm Module
10.03	Direction	Request
11.02	EXT1/EXT2 Select	Ext2
11.06	EXT REF2 Select	Comm Module
16.01	Run Enable	DI3
16.04	Fault Reset Select	Comm Module
20.01	Minimum Speed	-1200rpm
20.02	Maximum Speed	1200rpm
20.03	Maximum Current	200%
20.04	Maximum Torque	270%
50.01	Pulse Number	1200PPR
50.03	Encoder Fault	Fault
50.05	Encoder Channel	Ch2
50.06	Speed Feedback Select	Encoder
98.01	Encoder Module	Yes
98.02	Comm Module Link	Fieldbus

Table 4: CCS Drive Parameters

Ratings:

**Ratings 690 V** The table below shows the nominal ratings for the 690 V range drive sections.

Type Marking	Nominal Ratings			Duty Cycle (10 s / 60 s)		Duty Cycle (1 min / 5 min)		Frame type	P <sub>loss</sub> kW	Air flow m <sup>3</sup> /h	Noise level dBA	Width mm	Weight kg	Notes
	S <sub>N</sub> kVA	P <sub>N</sub> kW	I <sub>2N</sub> A	I <sub>2base</sub> A	I <sub>2max</sub> A	I <sub>2base</sub> A	I <sub>2max</sub> A							
Drive sections (525...690 V Range, U <sub>N</sub> = 690 V)														
ACA 610-09/00/00-6	9	5.5	7.6	6.2	12	6.2	9	R3I	0,14	60	48	400	170	1
ACA 610-09/09/00-6								2xR3I	0,28	120	50	400 or 600	210	1, 6
ACA 610-09/09/09-6								3xR3I	0,42	180	51	400 or 600	220	1, 6
ACA 610-11/00/00-6	11	8	10	8.7	17	8.7	13	R3I	0,17	60	48	400	170	1
ACA 610-11/11/00-6								2xR3I	0,34	120	50	400 or 600	210	1, 6
ACA 610-11/11/11-6								3xR3I	0,51	180	51	400 or 600	220	1, 6
ACA 610-16/00/00-6	16	11	14	10	20	10	15	R3I	0,24	60	48	400	170	1
ACA 610-16/16/00-6								2xR3I	0,48	120	50	400 or 600	210	1, 6
ACA 610-16/16/16-6								3xR3I	0,72	180	51	400 or 600	220	1, 6
ACA 610-20/00/00-6	20	15	20	15	30	15	23	R3I	0,30	60	48	400	170	1
ACA 610-20/20/00-6								2xR3I	0,60	120	50	400 or 600	210	1, 6
ACA 610-20/20/20-6								3xR3I	0,90	180	51	400 or 600	220	1, 6
ACA 610-025/000-6	25	19	25	20	40	20	30	R4I	0,38	70	54	400	240	1, 6
ACA 610-025/025-6								2xR4I	0,76	140	54	400 or 600	190	1
ACA 610-030/000-6	30	22	28	25	50	25	38	R4I	0,45	100	54	400	240	1, 6
ACA 610-030/030-6								2xR4I	0,90	200	54	400 or 600	190	1
ACA 610-040/000-6	40	30	36	28	56	28	42	R5I	0,60	260	54	400	240	1, 6
ACA 610-040/040-6								2xR5I	1,20	520	54	400 or 600	190	1
ACA 610-050/000-6	50	37	44	36	72	36	54	R5I	0,75	260	54	400	240	1, 6
ACA 610-050/050-6								2xR5I	1,50	520	54	400 or 600	190	1
ACA 610-060/000-6	60	45	52	44	88	44	66	R6I	0,90	480	64	400	200	1
ACA 610-060/060-6								2xR6I	1,80	960	68	600	250	1
ACA 610-070/000-6	70	55	65	52	104	52	78	R6I	1,05	480	64	400	200	1
ACA 610-070/070-6								2xR6I	2,10	960	68	600	250	1
ACA 610-100/000-6	100	75	88	65	130	65	98	R7I	1,50	480	64	400	200	1
ACA 610-100/100-6								2xR7I	3,00	960	68	600	250	1
ACA 610-120/000-6	120	90	105	88	176	88	132	R7I	1,80	480	64	400	200	1
ACA 610-120/120-6								2xR7I	3,60	960	68	600	250	1
ACA 610-0185-6	180	132	149	106	212	112	168	R8I	2,70	1550	61	600	250	2
ACA 610-0205-6	210	160	176	127	254	132	198	R8I	3,15	1550	61	600	250	2
ACA 610-0255-6	250	200	210	150	300	158	236	R8I	3,75	1550	61	600	250	2
ACA 610-315-6	310	250	264	179	358	198	297	R8I	4,65	1550	61	600	250	2
ACA 610-375-6	370	315	310	225	450	233	349	R9I	5,55	1550	61	600	270	2
ACA 610-0485-6	490	400	410	265	530	308	461	R9I	7,35	1550	61	600	270	2
ACA 610-600-6	600	500	502	340	680	377	565	R10I	9,00	3100	66	1000	450	2
ACA 610-0750-6	750	630	630	428	856	473	709	R11I	11,25	3100	66	1000	480	2
ACA 610-900-6	900	-	755	504	1008	568	849	R11I	13,50	3100	66	1000	480	2
ACA 610-1045-6	1040	-	874	644	1282	656	982	R12I	15,80	4650	69	1500	950	3
ACA 610-1385-6	1380	-	1158	755	1510	867	1301	R12I	20,70	4650	69	1500	950	3
ACA 610-1710-6	1710	-	1435	1007	2014	1076	1614	2xR11I	25,65	6200	69	2x1000	1200	3, 5
ACA 610-2125-6	2120	-	1777	1283	2566	1333	1999	2xR12I	31,80	9300	71	2x1500	1900	4
ACA 610-2545-6	2540	-	2129	1511	3022	1597	2395	2xR12I	38,10	9300	71	2x1500	1900	4
ACA 610-2800-6	2900	-	2344	1710	3420	1758	2637	4xR11I	42,00	12400	71	4x1000	2400	4
ACA 610-3350-6	3350	-	2809	2014	4028	2107	3160	4xR11I	50,25	12400	71	4x1000	2400	4
ACA 610-3890-6	3890	-	3251	2564	5128	2438	3657	4xR12I	58,20	18600	72	4x1500	3800	4
ACA 610-5140-6	5140	-	4300	3020	6040	3225	4838	4xR12I	77,10	18600	72	4x1500	3800	4

Table 5: ABB ACS600 Drive Rating [28]

### C. Motor Information

Description	Data
Machine type code	HXR 400LJ6
Machine type	Squirrel cage motor
Mounting designation	Horizontal
Protected by enclosure	TEAO
Method of cooling	TEAO
Insulation	Class F
Service factor	1.15 @ 115 °C RES
Standards	NEMA, CSA
Ambient temperature, max.	40 °C
Altitude, max.	3300 ft.a.s.l.
Converter Supply	ACS
Duty type	Continuous
Rated output	643hp
Voltage	660V
Frequency	60Hz
Speed	1200rpm
Current	549A
Connection of stator winding	Delta
Direction of rotation	Bi-directional
Sound pressure level (conv. supply, no load)	85 dBA, tol. + 3 dBA, 3 ft
Inertia rotor	Approx. 590 lb-ft <sup>2</sup>
Bearings	Antifriction

Table 6: CCS ABB Motor Information